Journal of Statistical Physics, Vol. 126, No. 1, January 2007 (© 2006)
DOI: 10.1007/s10955-006-9234-4

Lattice Boltzmann modeling with discontinuous collision components: Hydrodynamic and Advection-Diffusion Equations

Irina Ginzburg

Received January 24, 2006, accepted October 9, 2006
Published Online: December 22, 2006

Irrespective of the nature of the modeled conservation laws, we establish first the microscopic interface continuity conditions for Lattice Boltzmann (LB) multiple-relaxation time, link-wise collision operators with discontinuous components (equilibrium functions and/or relaxation parameters). Effective macroscopic continuity conditions are derived for a planar *implicit interface* between two immiscible fluids, described by the simple two phase hydrodynamic model, and for an *implicit interface boundary* between two heterogeneous and anisotropic, variably saturated soils, described by Richard's equation. Comparing the effective macroscopic conditions to the physical ones, we show that the range of the accessible parameters is restricted, e.g. a variation of fluid densities or a heterogeneity of the anisotropic soil properties. When the interface is *explicitly* tracked, the interface collision components are derived from the leading order continuity conditions. Among particular interface solutions, a harmonic mean value is found to be an exact LB solution, both for the interface kinematic viscosity and for the interface vertical hydraulic conductivity function. We construct simple problems with the explicit and implicit interfaces, matched exactly by the LB hydrodynamic and/or advection-diffusion schemes with the aid of special solutions for free collision parameters.

KEY WORDS: Lattice-Boltzmann equation, Interface conditions, Immiscible fluids, Hydrodynamic models, Diffusion and convection, Heterogeneity, Anisotropy, Layered porous media, Richards' equation.

1. INTRODUCTION

We study the interface properties of the Lattice Boltzmann (LB) schemes both for the microscopic two phase (Navier-Stokes) flows and the macroscopic (Darcy's)

[1] Cemagref, Antony Regional Centre, HBAN, Parc de Tourvoie - BP 44, 92163 Antony cedex, France. e-mail: irina.ginzburg@cemagref.fr

flows in heterogeneous anisotropic aquifers. Despite the apparent difference of the resolved equations, both problems share a common numerical feature, namely the discontinuity of their coefficients and macroscopic derivatives on the interfaces. LB methods have been applied to multi-phase hydrodynamics since the end of the eighties. The reader can find overviews of the main approaches in Rothman and Zaleski,[51] Chen and Doolen,[7] Pan et al.[43] and Raabe.[46] The analysis of two phase schemes is focused mostly on two principal components: the modeling of surface tension and the modeling of phase propagation, both are crucial for the physical description of the interface behavior. Therefore, the *effective continuity relations* obtained on an immobile interface between two immiscible fluids is perhaps a trivial question.

However, even for a planar interface in the absence of surface tension, one could ask the question about how the *microscopic* and *macroscopic* continuity relations are imposed *implicitly* by the LB scheme. The answer is not trivial since the Chapman-Enskog analysis[9,12] does not apply automatically when the derivatives of the conserved quantities and/or the collision components undergo jumps. The LB schemes carry distinct kinematic and bulk viscosities with the discontinuous relaxation parameters of their collision operators. The pressure continuity condition results in discontinuous coefficients of the equilibrium functions when the densities of the two fluids differ, at least for the simplest two phase models.[41,55,56] We are not aware of any analysis of the continuity relations for velocity and normal shear stress tensor components except for the free interface LB methods[21,36] where they are imposed explicitly.

The present work extends former analysis[17] for two principal interface approaches. The first reflects an *implicit* interface tracking, where the effective interface location is not relevant for execution of the algorithm. In this paper the extreme situation is addressed, when the collision operator assigned for one of two phases (say, "red") is applied to grid nodes lying below an imaginary interface and another operator, (say, "blue") which is applied for grid nodes lying above, regardless of the effective phase distribution. For example, the choice of the collision operator with a *majority* rule results in a simplified two phase handling for the immobile flat interface. The question then is what the interface continuity relations are for the velocity and viscous stress components and where are they satisfied.

The second configuration addresses *explicit* interface tracking. Here, "blue" and "red" operators are applied above and below grid nodes where a special *interface* collision operator is applied. One usually imagines that this corresponds to a less rough treatment of the grid nodes where the two phases coexist. The question then is how to define the interface collision components (the equilibrium functions and relaxation rates). We look for interface collision operators which maintain the interface continuity conditions in the most accurate way at the prescribed interface position.

For the modeling of stratified (layered) soils, the interface (boundary) position within or between mesh nodes is selected *a priori*. Variably saturated macroscopic flow is described by the highly non-linear, parabolic type Richard's equation. Its modeling represents a difficult numerical task.[6,39] The LB schemes have recently been extended in Refs. 25, 26 for Richard's equation in heterogeneous anisotropic aquifers. They are based on the LB approaches[23,57,58] for the anisotropic advection-diffusion equations (AADE). Although the normal component of the advective-diffusive flux (Darcy's velocity) is continuous on the interfaces, the conserved mass quantity (volumetric water content) and pressure gradients undergo jumps on the interfaces when the two soils have different retention or conductive behavior. The collision components (the relaxation parameters and/or the equilibrium functions) become discontinuous on the soil interfaces when the conductive and/or anisotropic properties vary. Saturated flow in heterogeneous anisotropic stratified aquifers, so called "groundwater whirls",[1] represents a "simple" convection-diffusion problem with discontinuous diagonal and off-diagonal elements of the diffusion tensors.

We first develop the LB framework for the uniform description of the hydrodynamic and AADE models. For this purpose we restrict ourselves to link-wise collision operators, with multiple relaxation times for the AADE and two relaxation times for the Navier-Stokes equations (NSE below). The latter restriction comes from an additional collision constraint, the momentum conservation. We then develop the analysis for the explicit and implicit interface descriptions. Effective continuity relations are first formulated in terms of the symmetric/anti-symmetric equilibrium and non-equilibrium solution parts. They are then restricted to NSE and AADE modeling. In particular, the first-order analysis shows how to select an interface collision operator for exact solutions, e.g. the piece-wise linear (Couette) flow in a straight channel or the vertical Darcy's flow in heterogeneous anisotropic media. The second-order analysis further restricts free collision components and enables exact piece-wise parabolic solutions, e.g. two phase Poiseuille flow with different viscosities and/or different forcing.

The paper is organized as follows. Section 2.1 presents the generic LB schemes based on the decomposition of the collision operator on symmetric and anti-symmetric parts. Section 2.2 adapts these schemes for the hydrodynamic equations and discusses the two phase modeling. Section 2.3 generalizes the AADE schemes from Ref. 23 and discusses the modeling of variably saturated Darcy's flow. Section 3 derives the generic interface relations for explicit and implicit tracking of planar interfaces. The interface relations are developed for the NSE in Sec. 4 and for the AADE in Sec. 5, they are demonstrated by exact solutions. Sub-sections 4.2.4 and 5.2.4 resume the obtained eigenvalue and equilibrium solutions for the explicit interfaces. Section 6 concludes the paper.

2. LATTICE BOLTZMANN SCHEMES

2.1. Evolution Equation

The unknown variable of the scheme is the population vector $\boldsymbol{f}(\vec{\mathbf{r}},t)=\{f_q,\quad q=0,\ldots,Q-1\}$ which is initialized at time $t=0$ on the nodes $\vec{\mathbf{r}}$ of an equidistant d-dimensional computational mesh. The evolution of the populations obeys the following update rule:

$$
\begin{aligned}
f_q(\vec{\mathbf{r}}+\vec{\mathbf{C}}_q,t+1)&=\tilde{f}_q(\vec{\mathbf{r}},t),\quad q=0,\ldots,Q-1,\\
\tilde{f}_q(\vec{\mathbf{r}},t)&=f_q(\vec{\mathbf{r}},t)+(\mathsf{A}\cdot\boldsymbol{f}^{\mathrm{ne.}})_q+\mathcal{Q}_q,\quad (\mathsf{A}\cdot\boldsymbol{f}^{\mathrm{ne.}})_q=p_q+m_q,\\
p_q&=\lambda_q^+\big(f_q^+-f_q^{\mathrm{eq.}+}\big),\quad m_q=\lambda_q^-\big(f_q^--f_q^{\mathrm{eq.}-}\big),\\
f_q^\pm&=\frac{1}{2}(f_q\pm f_{\bar{q}}),\quad \vec{\mathbf{C}}_q=-\vec{\mathbf{C}}_{\bar{q}}.
\end{aligned}
\tag{1}
$$

The velocity set contains Q vectors: one zero, $\vec{\mathbf{C}}_0=\vec{\mathbf{0}}$, for the rest population, and $Q-1$ non-zero ones, $\vec{\mathbf{C}}_q=\{C_{q\alpha},\quad \alpha=1,\ldots,d\}$, $q=1,\ldots,Q-1$, for the moving populations. Each non-zero velocity vector has a diametrically opposite one. Below we refer to a pair of anti-parallel velocities $(\vec{\mathbf{C}}_q,\vec{\mathbf{C}}_{\bar{q}})$ as to *a link*. A pair of velocities parallel to the main coordinate axes will be referred to as a *coordinate link*. Other velocity pairs are labeled as *diagonal links*. For the coordinate links, $C_{q\alpha}C_{q\beta}\equiv 0$ if $\alpha\neq\beta$ and for the *diagonal links*, $C_{q\alpha}C_{q\beta}\neq 0$ at least for the one pair $\alpha\neq\beta$.

The linear collision operator, $(\mathsf{A}\cdot\boldsymbol{f}^{\mathrm{ne.}})$, acts on the non-equilibrium part of the population, $\boldsymbol{f}^{\mathrm{ne.}}=\{f_q^{\mathrm{ne.}}\}=\{f_q-f_q^{\mathrm{eq.}}\}$. The operator is specified on a link (L-)basis. Projection of vector $\boldsymbol{f}$ on to the L-basis vectors are equal to its symmetric (even) and anti-symmetric (odd) counterparts: $f_q=f_q^++f_q^-$. The even parts are equal for a pair of populations with anti-parallel velocities, $f_q^+=f_{\bar{q}}^+$, and the odd parts have opposite signs, i.e. $f_q^-=-f_{\bar{q}}^-$. The source term $\mathcal{Q}_q$ is also decomposed into symmetric and anti-symmetric parts, $\mathcal{Q}_q=\mathcal{Q}_q^++\mathcal{Q}_q^-$. We restrict ourselves to the forcing $\vec{\mathbf{F}}$ (only) for the NSE and the mass source M (only) for the AADE:

$$
\begin{aligned}
&\text{NSE:}\quad \mathcal{Q}_q=\mathcal{Q}_q^-,\quad \mathcal{Q}_q^+=0,\quad \vec{\mathbf{F}}=\sum_{q=1}^{Q-1}\mathcal{Q}_q^-\vec{\mathbf{C}}_q,\\
&\text{AADE:}\quad \mathcal{Q}_q=\mathcal{Q}_q^+,\quad \mathcal{Q}_q^-=0,\quad M=\sum_{q=0}^{Q-1}\mathcal{Q}_q^+.
\end{aligned}
\tag{2}
$$

The mass variable, s, is defined as the sum of the population solution, i.e. $s=\sum_{q=0}^{Q-1}f_q$. The mass conserving equilibrium $\boldsymbol{f}^{\mathrm{eq.}}=\{f_q^{\mathrm{eq.}}\}$ is first written as:

$$
f_q^{\mathrm{eq.}}=f_q^{\mathrm{eq.}+}+f_q^{\mathrm{eq.}-},\quad q=0,\ldots,Q-1,
$$

$$
\begin{aligned}
f_q^{\text{eq.}-} &= t_q^\star J_q, \quad J_q = (\vec{\mathbf{J}} \cdot \vec{\mathbf{C}}_q), \quad q = 0, \ldots, Q-1, \\
f_q^{\text{eq.}+} &= \bar{\mathcal{D}}(s) E_q, \quad q = 1, \ldots, Q-1, \\
f_0^{\text{eq.}+} &= f_0^{\text{eq.}} = s - \sum_{q=1}^{Q-1} f_q^{\text{eq.}+} = s - \bar{\mathcal{D}}(s) \sum_{q=1}^{Q-1} E_q.
\end{aligned} \tag{3}
$$

"Odd" components $f_q^{\text{eq.}-}$ are proportional to projection of a d-dimensional vector $\vec{\mathbf{J}}$ on to the velocity vectors $\vec{\mathbf{C}}_q$. The weights $t_q^\star$ are *isotropic*, i.e. they have one value per velocity class $p = |\vec{\mathbf{C}}_q|$ and

$$
\sum_{q=1}^{Q-1} t_q^\star C_{q\alpha} C_{q\beta} = \delta_{\alpha\beta}, \quad 3 \sum_{q=1}^{Q-1} t_q^\star C_{q\alpha}^2 C_{q\beta}^2 = 1, \quad \alpha \neq \beta. \tag{4}
$$

Thus $\{t_1^\star = \frac{1}{3}, t_2^\star = \frac{1}{12}\}$ for $d2Q9$, $\{t_2^\star = \frac{1}{8}\}$ for $d3Q13$, $\{t_1^\star = \frac{1}{3}, t_3^\star = \frac{1}{24}\}$ for $d3Q15$, $\{t_1^\star = \frac{1}{6}, t_2^\star = \frac{1}{12}\}$ for $d3Q19$, following.[13,42] The equilibrium variable $\bar{\mathcal{D}}(s)$ is either a linear or a non-linear function of the conserved quantities. The symmetric "weight" functions E_q may represent any arbitrary function of the conserved quantities and external components, e.g., the advection-velocity or the source terms.

The macroscopic behavior is usually obtained with the help of the Chapman-Enskog expansion,[9,12] which develops the microscopic conservation relations up to second order about the equilibrium, in terms of a small parameter ε, $\varepsilon = 1/L$, L being a characteristic length. The Chapman-Enskog analysis is much easier to obtain in a consistent way when the first, second and any next order term of the expansion does not have any projections on to the conserved vectors. Although the source term can be incorporated, totally or partially, into the equilibrium function, which leads to equivalent forms of the evolution equation based on non-conserving equilibrium functions, it is important to note that the equilibrium function contains the conserved quantities in this paper. The mass conservation solvability condition of the evolution equation implies that the post-collision population part has no mass, provided that all "even" eigenvalues λ_q^+ are equal and that "odd" eigenvalues λ_q^- are equal link-wise:

$$
\begin{aligned}
\text{NSE, AADE}: \; s = \sum_{q=0}^{Q-1} f_q = \sum_{q=0}^{Q-1} f_q^{\text{eq.}}, \quad \sum_{q=0}^{Q-1} p_q = 0, \\
\lambda_q^+ = \lambda_e, \quad \lambda_q^- = \lambda_{\bar{q}}^-, \quad q = 0, \ldots, Q-1.
\end{aligned} \tag{5}
$$

For the hydrodynamic equation, conservation of momentum is required:

$$\text{NSE}: \vec{\mathbf{J}} = \sum_{q=1}^{Q-1} f_q \vec{\mathbf{C}}_q = \sum_{q=1}^{Q-1} f_q^{\text{eq.}} \vec{\mathbf{C}}_q, \quad \sum_{q=1}^{Q-1} m_q \vec{\mathbf{C}}_q = 0,$$

$$\lambda_q^- = \lambda_{\bar{q}}^- = \lambda_o, \quad \forall\, q = 1, \ldots, \frac{Q-1}{2}. \tag{6}$$

For both NSE and AADE, the post-collision counterparts p_q and m_q can therefore be computed once for each link:

$$p_q = p_{\bar{q}}, \quad m_q = -m_{\bar{q}}, \quad \vec{\mathbf{C}}_q = -\vec{\mathbf{C}}_{\bar{q}}. \tag{7}$$

The eigenvalue functions $\Lambda(\lambda) = -(\frac{1}{2} + \frac{1}{\lambda}), \forall\, \lambda$ will be labeled as:

$$\text{NSE, AADE}: \ \Lambda_e = \Lambda(\lambda_e),$$

$$\text{NSE}: \ \Lambda_q = \Lambda_o = \Lambda(\lambda_o), \quad \lambda_q^- = \lambda_{\bar{q}}^- = \lambda_o, \quad \forall\, q = 1, \ldots, \frac{Q-1}{2},$$

$$\text{AADE}: \ \Lambda_q = \Lambda(\lambda_q^-), \quad \lambda_q^- = \lambda_{\bar{q}}^-, \quad \forall\, q = 1, \ldots, \frac{Q-1}{2}. \tag{8}$$

With this notation, one can represent the population solution and its post-collision values as:

$$f_q(\vec{\mathbf{r}}) = f_q^{\text{eq.}+} + f_q^{\text{eq.}-} - \left[\frac{1}{2} + \Lambda_e\right] p_q - \left[\frac{1}{2} + \Lambda_q\right] m_q, \quad \forall q,$$

$$\tilde{f}_q(\vec{\mathbf{r}}) = f_q^{\text{eq.}+} + f_q^{\text{eq.}-} + \left[\frac{1}{2} - \Lambda_e\right] p_q + \left[\frac{1}{2} - \Lambda_q\right] m_q + \mathcal{Q}_q, \quad \forall q. \tag{9}$$

All eigenvalues λ are restricted to the linear stability interval: $-2 < \lambda < 0$ such that $\Lambda(\lambda) > 0, \forall \lambda$. The *two-relaxation-time* TRT-operator with two eigenvalues, λ_e and λ_o, is suitable for both mass and momentum conservation laws. The TRT-operator is thus a particular form of the multiple-relaxation-time MRT−operator.[12,14] The MRT−operator reduces to the TRT-operator when the eigenvalues are equal to λ_e for all even eigenvectors, and equal to λ_o for all odd eigenvectors. The TRT-operator does not, therefore, have any "macroscopic" advantage over the MRT-operator but does so for the computational efficiency and simplicity of the analysis and coding. Also, the link based approach naturally incorporates the multi-reflexion type boundary conditions.[2,22,24,44] The BGK-operator[42] is a particular form of the TRT-operator when $\lambda_e = \lambda_o$ and has a single relaxation parameter $\tau = -\frac{1}{\lambda_e} = -\frac{1}{\lambda_o}$. Besides an advanced computational efficiency (since one of two eigenvalues is free and can be used to improve for the stability and the higher order accuracy), the TRT model has some "macroscopic" advantages over the BGK one. In particular, the TRT-operator conserves momentum independently of the even (viscosity) eigenvalues. Two phase LB models may then avoid an

artificial construction of the equilibrium momentum value for fluids with different viscosities (e.g, BGK models).[43,49] The anisotropic diffusion equations can be modeled with the mass conserving equilibrium functions, since the equilibrium mass value can be assigned independently of the diffusion (odd) eigenvalues, which is in contrast to the BGK AADE models.[57,58]

2.2. Hydrodynamic Equations (NSE)

2.2.1. One Phase

We fit rel. (3) to the NSE equilibrium function assuming that the fluid density, ρ, and the macroscopic momentum, $\vec{\mathbf{j}}$, are given by:

$$\begin{aligned}
&\rho = s, \quad \bar{\mathcal{D}}(s) = P(\rho), \quad P(\rho) = c_s^2 \rho, \\
&E_q = t_q^\star \left(1 + \frac{1}{c_s^2} E_q^{(u)}(\vec{\mathbf{u}})\right), \quad E_q^{(u)}(\vec{\mathbf{u}}) = \frac{(3u_q^2 - u^2)}{2}, \\
&\vec{\mathbf{u}} = \frac{\vec{\mathbf{j}}}{\rho}, \quad \vec{\mathbf{j}} = \vec{\mathbf{J}} + \frac{1}{2}\vec{\mathbf{F}}, \quad u_q = (\vec{\mathbf{u}} \cdot \vec{\mathbf{C}}_q), \quad u^2 = \sum_{\alpha=1}^{d} u_\alpha^2,
\end{aligned} \tag{10}$$

where c_s^2 is a free parameter. The correction $\vec{\mathbf{F}}$ for the total momentum $\vec{\mathbf{J}}$ was first introduced for the MRT models[1,18,21,22,34] where the projections on the lattice velocities $\vec{\mathbf{C}}_\alpha$ represent the conserved quantities. For the TRT collision operator, the equivalent form is:

$$f_q^{\text{eq.}-} = t_q^\star (\vec{\mathbf{j}} \cdot \vec{\mathbf{C}}_q), \quad \mathcal{Q}_q^- \to \mathcal{Q}_q^- + \frac{\lambda_o}{2} t_q^\star (\vec{\mathbf{F}} \cdot \vec{\mathbf{C}}_q), \quad q = 1, \ldots, Q-1. \tag{11}$$

This form reduces to the BGK form[4] (see Eq. (19) taking $\tau = -\frac{1}{\lambda_o}$ and $\mathcal{Q}_q^- = t_q^\star(1 + \frac{\lambda_o}{2})(\vec{\mathbf{F}} \cdot \vec{\mathbf{C}}_q)$). If necessary, the equilibrium distribution can include *even order* corrections of the forcing term (Eq. (20) in Ref. 29), but one replaces τ with $-\frac{1}{\lambda_e}$ for the symmetric terms.

Use of proportional weights for the pressure and momentum variables simplifies the *link-wise* coupling of the pressure gradients, momentum gradients and forcing terms in the solution expansion of the populations. This choice, however, may happen not to be the most stable (see Refs. 14, 37). The "incompressible" variants[9,11] replace $\frac{P}{c_s^2} E_q^{(u)}(\vec{\mathbf{u}})$ by $\rho_0 E_q^{(u)}(\vec{\mathbf{u}})$. The non-linear term $E_q^{(u)}(\vec{\mathbf{u}})$ vanishes for the Stokes equation.

The Chapman-Enskog analysis[9] of the solvability conditions (5) and (6) is developed for the MRT hydrodynamic models in Refs. 12, 13, 21, assuming that the second order pressure gradients and force gradients are at least of order $O(\varepsilon^3)$. Replacing relevant (entering into the transport coefficients) even eigenvalues by

λ_e, one can use the MRT hydrodynamic equations for the TRT and BGK models:

$$\partial_t \rho + \nabla \cdot \vec{\mathbf{j}} = O(\varepsilon^3),$$

$$\partial_t \vec{\mathbf{j}} + \nabla \cdot \left(\frac{\vec{\mathbf{j}} \otimes \vec{\mathbf{j}}}{\rho} \right) = -\nabla P + \nabla \cdot (\nu \nabla \vec{\mathbf{j}}) + \nabla(\nabla \cdot \nu_\xi \vec{\mathbf{j}}) + \vec{\mathbf{F}} + O(\varepsilon^3),$$

$$\nu = \frac{1}{3}\Lambda_e, \quad \nu_\xi = (\nu(2 - 3\mathcal{C}) + \xi),$$

$$\xi = (\mathcal{C} - c_s^2)\Lambda_e, \quad \mathcal{C} = \frac{d+2}{3d}. \tag{12}$$

The kinematic viscosity ν and the bulk viscosity ν_ξ are valid for $d2Q9$, $d3Q15$ and $d3Q19$ models. The $d3Q13$ model is presented in Ref. 13. The deficiency of the TRT and the BGK collisions for the compressible regime is that both viscosities are defined via one eigenvalue.

Assuming the characteristic velocity, U, be $O(\varepsilon)$, the density fluctuation around its average value ρ_0 is of second order in terms of the Mach number, Ma:

$$\rho = \rho_0(1 + \mathrm{Ma}^2 P'), \quad P' = \frac{P(\rho) - P(\rho_0)}{\rho_0 U^2}, \quad \mathrm{Ma} = \frac{U}{c_s}. \tag{13}$$

When $\mathrm{Ma}^2 P'$ is neglected, Eq. (12) takes the form of the incompressible NSE:

$$\nabla \cdot \vec{\mathbf{j}} = 0,$$

$$\rho_0 \partial_t \vec{\mathbf{u}} + \rho_0 \nabla \cdot (\vec{\mathbf{u}} \otimes \vec{\mathbf{u}}) = -\nabla P + \nabla \cdot (\mu \nabla \vec{\mathbf{u}}) + \vec{\mathbf{F}} + O(\varepsilon^3), \quad \mu = \rho_0 \nu. \tag{14}$$

2.2.2. Two Phases

The single phase Navier-Stokes solver is one component of any multi-phase scheme. Two other principal components are the modeling of the surface tension and the modeling of the phase propagation. Below we derive the continuity relations first in a generic form, suitable for any equilibrium distribution and for any source term. Expanding them, one may include the surface tension term, either via the symmetric equilibrium part (e.g., for the momentum conserving perturbation term[19,28,30,55] or for the free-energy formulation[5,33,50]), or via the forcing term, for the models with "intermolecular interactions".[32,43,48] A study of the impact of the perturbation term on the derived continuity relations (in Ref. 19) gives one example.

The choice of the advection scheme is conditioned by the selected phase description and desired structure (thickness) of the interfaces. "Kinetic" type schemes employ the convection-diffusion LB schemes to propagate the mass fraction variables[5,50] or the index function.[31] "Recoloring type" schemes[19,21,28,30,55] typically yield extremely sharp (one-two lattice units) interfaces. The effective

diffusion (anti-diffusion) coefficients may depend on the implementation details and they are difficult to derive (see Ref. 35). The schemes in Refs. 45, 47 try to control the interface width. The continuity analysis below does not need to specify the advection scheme but assumes that it is able to produce and maintain, for a flat interface, the two configurations described below.

Let us use the historical "color" notation for two fluids: "red" (R) and "blue" (B). Let $i^{(R)}(\vec{\mathbf{r}}, t)$ be the phase indicator, such that the (R)-collision operator is applied when $i^{(R)} = 1$ and the (B)-collision operator is applied when $i^{(R)} = 0$. Red and blue operators can have different equilibrium "weight" parameters, relaxation parameters and forcing terms. To complete the model, one needs to describe the collision components (equilibrium functions and relaxation parameters) for the nodes where two phases coexist, then $0 < i^{(R)} < 1$.

The analysis below treats two collision configurations. The first one, referred to as *an implicit interface*, is handled with only two collision operators, (R) and (B), and one of them is selected at the nodes where two fluids coexist. The decision argument here is the majority of the occupying phases: (R) if $i^{(R)} \geq i^{(B)}$ and (B) otherwise. This situation is sketched in Fig. 1. The second configuration, referred to as *an explicit interface*, is handled with three collision operators, (R), (B) and interface (I). This situation is sketched in Fig. 2. The analysis below aims to build the (I)-operator from the prescribed continuity relations and to relate the conserved equilibrium interface moments to their macroscopic "equivalents".

Our computations are performed with the reformulated model of Gunstensen et al.[28] In contrast to the original scheme, we operate with only one kind of the populations which obey the evolution Eq. (1). The phase distribution is represented with one additional variable, the mass fraction of one of the two fluids, say $\rho^{(R)}(\vec{\mathbf{r}}, t)$, then $i^{(R)} = \rho^{(R)}/\rho$. The phase update is computed as:

$$\rho^{(R)}(\vec{\mathbf{r}}, t+1) = \delta_0 \rho^{(R)}(\vec{\mathbf{r}}, t) + \sum_{q=1}^{Q-1} \delta_q \rho^{(R)}(\vec{\mathbf{r}} - \vec{\mathbf{C}}_q, t), \tag{15}$$

where $\delta_q \rho^{(R)}$, $q = 0, \ldots, Q-1$ is a solution of the "recoloring" scheme which preferentially redirects each fluid to the neighboring sites of the same "color", constrained by the local mass conservation: $\sum_{q=0}^{Q-1} \delta_q \rho^{(R)} = \rho^{(R)}(\vec{\mathbf{r}}, t)$. Further details can be found in Ref. 21.

The analysis is restricted to a planar interface $z = const$. Mass conservation is maintained on the *material* interface (where there is no mass exchange with the surrounding bulk phases) when both the normal and tangential *mass averaged velocities* are continuous on the interface (see, e.g., in Refs. 8, 10). Assuming a constant density for each bulk fluid, the velocity is continuous on the interface:

$$u_\alpha^{(R)} = u_\alpha^{(B)} = u_\alpha^{(I)}, \quad \alpha = \{x, y, z\}. \tag{16}$$

In the absence of surface forces, and for a *material interface* with no mass, the balance of the momentum for Eq. (12) becomes:

$$\begin{cases} P^{(R)} - 2\nu^{(R)}\partial_z j_z^{(R)} = P^{(B)} - 2\nu^{(B)}\partial_z j_z^{(B)}, \\ \nu^{(R)}\mathcal{D}_{\alpha z}^{(R)} \qquad\qquad = \nu^{(B)}\mathcal{D}_{\alpha z}^{(B)}, \quad \mathcal{D}_{\alpha z} = (\partial_\alpha j_z + \partial_z j_\alpha). \end{cases} \tag{17}$$

In the incompressible limit, these relations are equivalent to the continuity of the normal and tangential components of the normal shear stress tensor:

$$\begin{cases} P^{(R)} - 2\mu^{(R)}\partial_z u_z^{(R)} = P^{(B)} - 2\mu^{(B)}\partial_z u_z^{(B)}, \\ \mu^{(R)} D_{\alpha z}^{(R)} \qquad\qquad = \mu^{(B)} D_{\alpha z}^{(B)}, \quad D_{\alpha z} = (\partial_\alpha u_z + \partial_z u_\alpha). \end{cases} \tag{18}$$

2.3. Anisotropic Advection-diffusion Equations (AADE)

2.3.1. Basic Techniques

Assuming that $\vec{\mathbf{J}}$ is an external advective vector in (3), the second order approximation of the solvability condition (5) takes the form of the advection-dispersion equation:

$$\partial_t s + \nabla\cdot\vec{\mathbf{J}} = \nabla\cdot\vec{\mathbf{D}} + M, \quad \vec{\mathbf{D}} = \{D_\beta = -(\mathbf{\Phi}\cdot\boldsymbol{C}_\beta)\}, \quad \beta = 1,\ldots,d$$
$$\mathbf{\Phi} = \{\Phi_q\} = -\Lambda_q m_q = -\Lambda_q(\partial_t f_q^{\text{eq.}-} + \partial_q\bar{\mathcal{D}}(s)E_q) + O(\varepsilon^2). \tag{19}$$

The tensor of the numerical diffusion associated with $\partial_q\partial_t f_q^{\text{eq.}-}$ (see Refs. 23, 26) can be removed for linear convection-diffusion equations with the help of the non-linear equilibrium term $t_q^\star s E_q^{(u)}(\vec{\mathbf{u}})$ (see rel. (10)) when $\bar{\mathcal{D}}(s) = s$, $\vec{\mathbf{J}} = \vec{\mathbf{u}}s$ and all eigenvalues λ_q^- are equal (TRT operator). When the "weight" functions E_q do not vary in space, the "pure" diffusion counter-part of the diffusive flux vector $-\vec{\mathbf{D}}$ becomes:

$$-D_\alpha = -\mathsf{D}_{\alpha\beta}\partial_\beta\bar{\mathcal{D}}(s), \quad \mathsf{D}_{\alpha\beta} = 2\sum_{q=1}^{(Q-1)/2}\mathcal{T}_q C_{q\alpha}C_{q\beta}, \quad \mathcal{T}_q = \Lambda_q E_q. \tag{20}$$

The inverse of this relation yields the solution, $\mathcal{T}_\alpha$, for the coordinate links and solution, $\mathcal{T}_q$, for the diagonal links:

$$\mathcal{T}_\alpha = \frac{1}{2}(\mathsf{D}_{\alpha\alpha} - s_{\alpha\alpha}), \quad s_{\alpha\alpha} = 2\sum_{q(diag)}\mathcal{T}_q C_{q\alpha}^2, \quad \alpha = 1,\ldots,d, \tag{21}$$

$$\mathcal{T}_q = \frac{1}{4}(s_d + \mathsf{D}_{xy}C_{qx}C_{qy}), \quad s_d = s_{\alpha\alpha} = s_{xy}, \quad \text{for } d2Q9, \tag{22}$$

$$\mathcal{T}_q = \frac{1}{8}\Big(s_d + \sum_{\alpha\neq\beta}\mathsf{D}_{\alpha\beta}C_{q\alpha}C_{q\beta}\Big), \quad s_d = s_{\alpha\alpha} = s_{\alpha\beta}, \quad \text{for } d3Q15, \tag{23}$$

$$\mathcal{T}_q = \frac{1}{4}(s_{\alpha\beta} + \mathsf{D}_{\alpha\beta}C_{q\alpha}C_{q\beta}), \quad s_{\alpha\beta} = \frac{s_{\alpha\alpha} + s_{\beta\beta} - s_{\gamma\gamma}}{2}, \quad \text{for } d3Q13, d3Q19. \tag{24}$$

The models based on coordinate stencils ($d2Q5$, $d3Q7$) yield $s_{\alpha\alpha} = 0$ and cannot handle the off-diagonal elements. The $d3Q13$ set has no coordinate links at all, and rel. (24) fixes $\mathcal{T}_q$ values for its 6 diagonal links (with $s_{\alpha\alpha} = \mathsf{D}_{\alpha\alpha}$). For the models with two velocity classes, $\{s_{\alpha\alpha}\}$ can be regarded as free parameters. The $d2Q9$ and $d3Q15$ have only one free parameter s_d. The $d3Q19$ has three free parameters, $s_{\alpha\alpha}$, $s_{\beta\beta}$ and $s_{\gamma\gamma}$. When $\{s_{\alpha\alpha}\}$ and the solution (21)–(24) for $\{\mathcal{T}_q\}$ are fixed, one can either specify E_q or prescribe Λ_q for each link. Two principal approaches are developed in Refs. 23, 24, 26. The first technique, referred to as the **TRT-E model**, combines the TRT-operator and the *anisotropic* equilibrium weights, $\{E_q\}$, (E-model). The second technique, referred to as the **(Link) L- model**, combines the anisotropic eigenvalue set $\{\Lambda_q\}$ with the *isotropic* equilibrium weights $E_q = c_e t_q^\star$, $c_e > 0$ is a free parameter, restricted only by the stability condition. Von Neumann stability analysis[15] finds the positivity of the weights $\{f_q^{\text{eq.}+}/s\}$ as a necessary stability condition only for the immobile population (at least in case of the diagonal tensors). If one requires the positivity for other weights, the condition $\{\mathcal{T}_q \geq 0\}$ confines the free parameters $s_{\alpha\alpha}$:

$$|\mathsf{D}_{\alpha\beta}| \leq s_{\alpha\beta}, \quad s_{\alpha\alpha} = (s_{\alpha\beta} + s_{\alpha\gamma}) \leq \mathsf{D}_{\alpha\alpha}, \quad \mathsf{D}_{\alpha\alpha} \geq 0, \tag{25}$$

and therefore, restricts the range of the off-diagonal elements:

$$|\mathsf{D}_{\alpha\beta}| \leq \min_{\alpha} \mathsf{D}_{\alpha\alpha}, \quad \text{for } d2Q9, d3Q15, \tag{26}$$

$$|\mathsf{D}_{\alpha\beta}| + |\mathsf{D}_{\alpha\gamma}| \leq \mathsf{D}_{\alpha\alpha}, \quad \text{for } d3Q13 \ \ d3Q19, \tag{27}$$

$$|\mathsf{D}_{\alpha\beta}| \leq \frac{1}{2}(\mathsf{D}_{\alpha\alpha} + \mathsf{D}_{\beta\beta} - \mathsf{D}_{\gamma\gamma}), \quad \text{for } d3Q13. \tag{28}$$

We discuss in Ref. 27 available positive definite anisotropic diffusion tensors for each velocity set.

2.3.2. Flow in Stratified Porous Media

We consider the modeling of macroscopic flow in stratified porous media. Assuming that the air phase is continuous and at atmospheric pressure, the flow velocity $\vec{\mathbf{u}}^{(i)}$ inside the i^{th} layer can be related to the capillary pressure, $\psi^{(i)}(\theta)$, via Darcy's law:

$$\partial_t \theta + \nabla \cdot \vec{\mathbf{u}}^{(i)} = q_s^{(i)}, \quad \vec{\mathbf{u}}^{(i)} = -\mathbf{K}^{(i)}(\nabla h^{(i)}(\theta) + \vec{\mathbf{1}}_z), \quad h^{(i)}(\theta) = -\frac{\psi^{(i)}(\theta)}{\rho_0 g}. \tag{29}$$

Pressure head distribution $h^{(i)}(\theta)$ is a given function of the moisture content variable $\theta^{(i)}(\vec{\mathbf{x}}, t)$, a relative volumetric part of a soil occupied by water. The examples of the retention curves are plotted in Fig. 11. The medium is saturated when $\theta^{(i)} = \theta_s^{(i)}$ and it is dry when $\theta^{(i)} = \theta_r^{(i)}$. In Eq. (29), $q_s^{(i)}$ is a mass source, $\vec{\mathbf{1}}_z$ is an upward unit vector, $K_{\alpha\beta}^{(i)} = K(h)K_{\alpha\beta}^{a(i)}$ where $K^{(i)}(h) = k^{(i)}\rho_0 g/\mu$ is the hydraulic conductivity function and $k^{(i)}\mathbf{K}^{a(i)}$ is the permeability tensor. For the saturated media $\theta^{(i)} \equiv \theta_s^{(i)}$ and Richard's Eq. (29) becomes:

$$\nabla \cdot K^{(i)}(\nabla h^{(i)} + \vec{1}_z) = 0, \quad K^{(i)}(h) \equiv K_s^{(i)}, \quad h^{(i)} \geq h_s^{(i)} = h^{(i)}(\theta_s^{(i)}). \quad (30)$$

Let $\mathcal{L} = L'/L$, $\mathcal{U} = U'/U$ and $\mathcal{T} = T'/T$ ($T = L/U$, $T' = L'/U'$) be ratios of the characteristic values for the length, velocity and time variables between the computational and physical variables. Let the diagonal components $\mathsf{L} = \mathrm{diag}(L_x, L_y, L_z)$ define the scaling factors for every direction with respect to the characteristic scaling $\mathcal{L}$ between the cuboid computational grid and orthorhombic discretization grid. On the computational grid, the variables are $t' = \mathcal{T}t$ and $\vec{\mathbf{x}}' = \mathcal{L}\mathsf{L} \cdot \vec{\mathbf{x}}$, and for each layer Richard's Equation (29) becomes:

$$\partial_{t'}\theta + \nabla' \cdot \vec{\mathbf{J}} = \nabla' \cdot \mathbf{K}' \cdot \nabla h' + M, \quad h' = \mathcal{L}h, \quad \vec{\mathbf{J}} = -\mathbf{K}'(h)\mathsf{L} \cdot \vec{\mathbf{1}}_z,$$
$$\mathbf{K}' = K'(h)\mathbf{K}^{\mathbf{a}'}, \quad K'(h) = \mathcal{U}K(h), \quad \mathbf{K}^{\mathbf{a}'} = \mathsf{L}\mathbf{K}^{\mathbf{a}}\mathsf{L}, \quad M = q_s/\mathcal{T}. \quad (31)$$

The Darcy velocity (in lattice units) is the sum of the advective and diffusive fluxes,

$$u'_\alpha = J_\alpha + \Phi_\alpha, \quad \Phi_\alpha = (\mathbf{\Phi} \cdot \mathbf{C}_\alpha), \quad \alpha = 1, \ldots, d. \quad (32)$$

The LB formulations[25,26] for Eq. (29) are based on the different physical meanings assigned to the equilibrium (diffusion) variable $\bar{\mathcal{D}}(s)$:

- The mixed, $\theta/h-$form solves the original Eq. (31): $s = \theta$, $\bar{\mathcal{D}}(s) = h'$.
- The moisture content, $\theta-$form fits Eq. (31) to Eq. (19) with $s = \bar{\mathcal{D}}(s) = \theta$ and the diffusion tensor $\vec{\mathbf{D}}_{\alpha\beta} = \partial_\theta h' \mathbf{K}'_{\alpha\beta}(\theta)$.
- The Kirchoff transform, $\theta/K-$form with $s = \theta$ results in constant coefficients of the diffusion tensor using $\bar{\mathcal{D}}(s) = \int_{-\infty}^{h'(\theta)} K'(h)dh$, then $\vec{\mathbf{D}}_{\alpha\beta} \equiv \mathbf{K}^{a'}{}_{\alpha\beta}$.
- The pressure head, $h-$form with $\bar{\mathcal{D}}(s) = h'$ and $s = s_0 + (h' - h'_0)/H^{\mathrm{eq.}}$ (s_0 and h'_0 are some constants), is suitable for steady state solutions to Eq. (31). The parameter $H^{\mathrm{eq.}}$ may accelerate convergence. Any of the formulations above can be switched to $h-$form for the saturated zone, using a regular continuation of the retention curves beyond the air entry value h_s. This is given by linear extrapolation: $h'(\theta) = h'_s + \partial_\theta h'(\theta_s)(\theta - \theta_s)$, then $s_0 = \theta_s$, $h'_0 = h'_s$ and $H^{\mathrm{eq.}} = \partial_\theta h'(\theta_s)$.

These formulations select the diffusion variable along the lines of the well known direct discretization schemes for Richard's equation: mixed and pressure-based form are discussed in Refs. 6, 39, the Kirchoff-transform based methods are developed in Ref. 52.

We will assume a horizontal interface $z = z^{(I)}$ between (R) and (B) soil layers. The pressure distribution $h(\vec{\mathbf{r}})$ and the normal component $u_z(\vec{\mathbf{r}})$ should be continuous on the interface. When the vertical components $K_{zz}^{(i)}$ are heterogeneous, the convective component $-\mathbf{K}^{(i)}\vec{\mathbf{1}}_z$ of the Darcy velocity is not continuous, and the continuity of the component $u_z^{(i)}$ and the continuity of the diffusive flux component $-\mathbf{K}^{(i)}\nabla h$ differ. On the other hand, the continuity of $u_z = u_z'^{(i)}/(\mathcal{U}L_z^{(i)})$ is not equivalent to the continuity of the computational variable $u_z'^{(i)}$ when the vertical refinement is not uniform (scale factors $L_z^{(i)}$ differ). For steady state solutions, one can divide equations (31) by the $L_z^{(i)}$-value in each i^{th} sub-domain, without changing the solution procedure (see Ref. 26). In what follows we will assume that the coefficients of the solved equations are adjusted, such that the interface continuity relations are:

$$\begin{aligned} h'^{(R)}(z^{(I)}) &= h'^{(B)}(z^{(I)}), \\ (J_z^{(R)} + \Phi_z^{(R)})(z^{(I)}) &= (J_z^{(B)} + \Phi_z^{(B)})(z^{(I)}). \end{aligned} \tag{33}$$

3. GENERIC INTERFACE RELATIONS

3.1. Assumptions

The analysis is based on the second-order steady state expansion of the non-equilibrium part:

$$\begin{aligned} &p_0 = 0, \quad m_0 = 0, \\ &p_q = p_q{}^{[1]} + p_q{}^{[2]} + O(\varepsilon^3), m_q = m_q{}^{[1]} + m_q{}^{[2]} + O(\varepsilon^3), \quad q = 1, \ldots, Q-1, \end{aligned} \tag{34}$$

where, with the help of the directional derivatives along $\vec{\mathbf{C}}_q$, $\partial_q\phi = \nabla\phi \cdot \vec{\mathbf{C}}_q = \sum_\alpha^d \partial_\alpha\phi \boldsymbol{C}_\alpha, \forall\, \phi$:

$$\begin{aligned} NSE:\ & m_q{}^{[1]} = \partial_q f_q^{\mathrm{eq}.+}, \quad p_q{}^{[1]} = \partial_q f_q^{\mathrm{eq}.-}, \\ & m_q{}^{[2]} = -\partial_q \Lambda_e p_q{}^{[1]} - \mathcal{Q}_q^-, \quad p_q{}^{[2]} = O(\varepsilon^3). \end{aligned} \tag{35}$$

$$\begin{aligned} AADE:\ & p_q{}^{[1]} = \partial_q f_q^{\mathrm{eq}.-}, \quad m_q{}^{[1]} = \partial_q f_q^{\mathrm{eq}.+}, \\ & p_q{}^{[2]} = -\partial_q \Lambda_q m_q{}^{[1]} - \mathcal{Q}_q^+, \quad m_q{}^{[2]} = O(\varepsilon^3). \end{aligned} \tag{36}$$

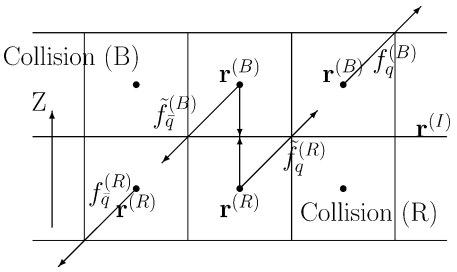

Fig. 1. Sketch for implicit interface tracking.

These relations follow from the generic form of the second order expansion, e.g. Eqs. (12–13) in Ref. 23, dropping the time derivatives. They can be obtained directly, by applying a Taylor series in space for the evolution Eq. (1). In agreement with the terms neglected for the macroscopic Eqs. (12) and (19), we neglect $p_q{}^{[2]}$ for the NSE, as related to the second derivatives of the pressure and third derivatives of the velocity, and $m_q{}^{[2]}$ for the AADE, as related to the second derivatives of the advective velocity and third derivatives of the diffusion variable. We restrict the analysis to an immobile interface:

$$j_z(\vec{\mathbf{r}}^{(I)}) = 0, \quad \partial_z j_z(\vec{\mathbf{r}}^{(I)}) = 0. \tag{37}$$

Although the analysis can be extended for more general situations, it should then incorporate a dynamic component which is responsible for the mass transfer. This depends on the actual advective algorithm and lies outside the scope of the present work.

3.2. Implicit Interface

We formulate and examine *implicit interface conditions* prescribed by the evolution Eq. (1) on an imaginary immobile flat interface between two distinct fluids (NSE) or two heterogeneous layers of porous media (AADE). We consider two grid nodes linked by a pair of anti-parallel velocities: $\vec{\mathbf{r}}^{(R)} = \vec{\mathbf{r}}^{(B)} + \vec{\mathbf{C}}_{\bar{q}}$ and $\vec{\mathbf{r}}^{(B)} = \vec{\mathbf{r}}^{(R)} + \vec{\mathbf{C}}_q$ (see sketch in Fig. 1):

$$\begin{cases} f_q(\vec{\mathbf{r}}^{(B)}, t+1) = \tilde{f}_q(\vec{\mathbf{r}}^{(R)}, t), & q \in I \\ \tilde{f}_{\bar{q}}(\vec{\mathbf{r}}^{(B)}, t) \quad\quad = f_{\bar{q}}(\vec{\mathbf{r}}^{(R)}, t+1), & \bar{q} \in \bar{I}. \end{cases} \tag{38}$$

We suppose that for each $\vec{\mathbf{C}}_q$, $\{q \in I\}$, there is an opposite velocity $\vec{\mathbf{C}}_{\bar{q}}$, $\{\bar{q} \in \bar{I}\}$, and vice-versa, and will call the link $\{\vec{\mathbf{C}}_q, \vec{\mathbf{C}}_{\bar{q}}\}$ an "interface" link. We impose the red (R) collision operator at $\vec{\mathbf{r}}^{(R)}$ and the blue (B) collision operator at $\vec{\mathbf{r}}^{(B)}$. Then, for the steady state, using the notation Φ_q for $-\Lambda_q m_q$ (cf. (19)) and taking into

account that $f_q^{\text{eq.}+} = f_{\bar{q}}^{\text{eq.}+}$, $f_q^{\text{eq.}-} = -f_{\bar{q}}^{\text{eq.}-}$, $p_q = p_{\bar{q}}$, $m_q = -m_{\bar{q}}$, $\Phi_q = -\Phi_{\bar{q}}$, substitution of rel. (9) into Eq. (38) gives:

$$\begin{cases} f_{\bar{q}}^{\text{eq.}+(B)} - f_{\bar{q}}^{\text{eq.}-(B)} - (\frac{1}{2} + \Lambda_e^{(B)}) p_{\bar{q}}^{(B)} + \frac{1}{2} m_{\bar{q}}^{(B)} - \Phi_{\bar{q}}^{(B)} \\ = f_q^{\text{eq.}+(R)} + f_q^{\text{eq.}-(R)} + (\frac{1}{2} - \Lambda_e^{(R)}) p_q^{(R)} + \frac{1}{2} m_q^{(R)} + \Phi_q^{(R)} + \mathcal{Q}_q^{(R)}, \\ f_{\bar{q}}^{\text{eq.}+(B)} + f_{\bar{q}}^{\text{eq.}-(B)} + (\frac{1}{2} - \Lambda_e^{(B)}) p_{\bar{q}}^{(B)} + \frac{1}{2} m_{\bar{q}}^{(B)} + \Phi_{\bar{q}}^{(B)} + \mathcal{Q}_{\bar{q}}^{(B)} \\ = f_q^{\text{eq.}+(R)} - f_q^{\text{eq.}-(R)} - (\frac{1}{2} + \Lambda_e^{(R)}) p_q^{(R)} + \frac{1}{2} m_q^{(R)} - \Phi_q^{(R)}. \end{cases} \tag{39}$$

The sum and difference of these equations yields two conditions per link:

$$\left[S_q^{(R)} + \frac{1}{2} \mathcal{Q}_q^{(R)} \right] (\vec{\mathbf{r}}^{(R)}) = \left[S_{\bar{q}}^{(B)} (\vec{\mathbf{r}}^{(B)}) + \frac{1}{2} \mathcal{Q}_{\bar{q}}^{(B)} \right] (\vec{\mathbf{r}}^{(B)}),$$

$$\text{with } S_q = f_q^{\text{eq.}+} + \frac{1}{2} m_q - \Lambda_e p_q, \tag{40}$$

$$\left[G_q^{(R)} + \frac{1}{2} \mathcal{Q}_q^{(R)} \right] (\vec{\mathbf{r}}^{(R)}) = - \left[G_{\bar{q}}^{(B)} + \frac{1}{2} \mathcal{Q}_{\bar{q}}^{(B)} \right] (\vec{\mathbf{r}}^{(B)}),$$

$$\text{with } G_q = f_q^{\text{eq.}-} + \Phi_q + \frac{1}{2} p_q. \tag{41}$$

Relations (39)–(41) rely only on the link-based form of the evolution equation. They are exact for any equilibrium distribution. Below we analyze them for the mid-point (interface point) $\vec{\mathbf{r}}^{(I)}$:

$$\vec{\mathbf{r}}^{(I)} = \vec{\mathbf{r}}^{(R)} + \frac{1}{2} \vec{\mathbf{C}}_q = \vec{\mathbf{r}}^{(B)} + \frac{1}{2} \vec{\mathbf{C}}_{\bar{q}}. \tag{42}$$

3.3. Explicit Interface

We assume that the interface grid node is located midway between two grid nodes $\vec{\mathbf{r}}^{(R)} = \vec{\mathbf{r}}^{(I)} + \vec{\mathbf{C}}_{\bar{q}}$ and $\vec{\mathbf{r}}^{(B)} = \vec{\mathbf{r}}^{(I)} + \vec{\mathbf{C}}_q$ (see sketch on Fig. 2). We impose the (R)-collision operator at $\vec{\mathbf{r}}^{(R)}$, the (B)-operator at $\vec{\mathbf{r}}^{(B)}$ and the interface (I)-collision operator at $\vec{\mathbf{r}}^{(I)}$. The propagation from $\vec{\mathbf{r}}^{(I)}$ to $\vec{\mathbf{r}}^{(B)}$ and $\vec{\mathbf{r}}^{(R)}$ gives two equations:

$$\begin{cases} \tilde{f}_q^{(I)} (\vec{\mathbf{r}}^{(I)}, t) & = f_q^{(B)} (\vec{\mathbf{r}}^{(B)}, t+1), \\ f_{\bar{q}}^{(R)} (\vec{\mathbf{r}}^{(R)}, t+1) & = \tilde{f}_{\bar{q}}^{(I)} (\vec{\mathbf{r}}^{(I)}, t), \qquad q \in I. \end{cases} \tag{43}$$

The propagation from $\vec{\mathbf{r}}^{(R)}$ and $\vec{\mathbf{r}}^{(B)}$ toward $\vec{\mathbf{r}}^{(I)}$ completes the system:

$$\begin{cases} f_q^{(I)} (\vec{\mathbf{r}}^{(I)}, t+1) = \tilde{f}_q^{(R)} (\vec{\mathbf{r}}^{(R)}, t) = f_q^{(R)} (\vec{\mathbf{r}}^{(I)}, t+1), \\ f_{\bar{q}}^{(I)} (\vec{\mathbf{r}}^{(I)}, t+1) = \tilde{f}_{\bar{q}}^{(B)} (\vec{\mathbf{r}}^{(B)}, t) = f_{\bar{q}}^{(B)} (\vec{\mathbf{r}}^{(I)}, t+1), \; q \in I. \end{cases} \tag{44}$$

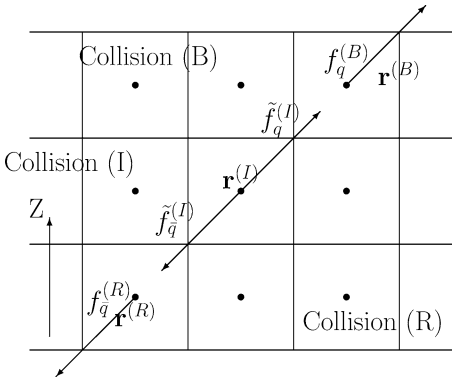

Fig. 2. Sketch for explicit interface tracking.

An immobile interface node will maintain the continuation of the bulk solutions if it acts as a "red" node for the populations leaving it for the red "layer" and as a "blue" node for the opposite one, i.e. when in (43):

$$\tilde{f}_q^{(I)}(\vec{\mathbf{r}}^{(I)},t)=\tilde{f}_q^{(B)}(\vec{\mathbf{r}}^{(I)},t),\quad \tilde{f}_{\bar{q}}^{(I)}(\vec{\mathbf{r}}^{(I)},t)=\tilde{f}_{\bar{q}}^{(R)}(\vec{\mathbf{r}}^{(I)},t),\quad q\in I. \tag{45}$$

At steady state, replacing $\tilde{f}_q^{(I)}(\vec{\mathbf{r}}^{(I)})$ by $f_q^{+(R)}+f_q^{-(R)}$, $f_{\bar{q}}^{(I)}(\vec{\mathbf{r}}^{(I)})$ by $f_{\bar{q}}^{+(B)}-f_q^{-(B)}$, Eq. (45) reads as:

$$\begin{aligned}
&f_q^{+(R)}+f_q^{-(R)}+\lambda_e^{(I)}f_q^{\mathrm{ne.}+(I)}+\lambda_q^{-(I)}f_q^{\mathrm{ne.}-(I)}+\mathcal{Q}_q^{(I)}=\\
&f_q^{+(B)}+f_q^{-(B)}+\lambda_e^{(B)}f_q^{\mathrm{ne.}+(B)}+\lambda_q^{-(B)}f_q^{\mathrm{ne.}-(B)}+\mathcal{Q}_q^{(B)},\\
&f_{\bar{q}}^{+(R)}+f_{\bar{q}}^{-(R)}+\lambda_e^{(R)}f_{\bar{q}}^{\mathrm{ne.}+(R)}+\lambda_q^{-(R)}f_{\bar{q}}^{\mathrm{ne.}-(R)}+\mathcal{Q}_{\bar{q}}^{(R)}=\\
&f_{\bar{q}}^{+(B)}-f_q^{-(B)}+\lambda_e^{(I)}f_q^{\mathrm{ne.}+(I)}-\lambda_q^{-(I)}f_q^{\mathrm{ne.}-(I)}+\mathcal{Q}_{\bar{q}}^{(I)},
\end{aligned} \tag{46}$$

$$\text{where}\quad f_q^{\mathrm{ne.}+(I)}=\frac{1}{2}(f_q^{(R)}+f_{\bar{q}}^{(B)})-f_q^{\mathrm{eq.}+(I)},$$

$$f_q^{\mathrm{ne.}-(I)}=\frac{1}{2}(f_q^{(R)}-f_{\bar{q}}^{(B)})-f_q^{\mathrm{eq.}-(I)}. \tag{47}$$

Using the notation $\lambda_q^{-(I)}f_q^{\mathrm{ne.}-(I)}=m_q^{(I)}$, $\lambda_e^{(I)}f_q^{\mathrm{ne.}+(I)}=p_q^{(I)}$, their sum and difference are, respectively:

$$m_q^{(I)}+\frac{1}{2}(\mathcal{Q}_q^{(I)}-\mathcal{Q}_{\bar{q}}^{(I)})=(S_q^{(B)}-S_{\bar{q}}^{(R)})(\vec{\mathbf{r}}^{(I)})+\frac{1}{2}(\mathcal{Q}_q^{(B)}-\mathcal{Q}_{\bar{q}}^{(R)})$$

$$\text{with } S_q=f_q^{\mathrm{eq.}+}+\frac{1}{2}m_q-\Lambda_e p_q, \tag{48}$$

$$p_q^{(I)} + \frac{1}{2}(\mathcal{Q}_q^{(I)} + \mathcal{Q}_{\bar{q}}^{(I)}) = (G_q^{(B)} + G_{\bar{q}}^{(R)})(\vec{\mathbf{r}}^{(I)}) + \frac{1}{2}(\mathcal{Q}_q^{(B)} + \mathcal{Q}_{\bar{q}}^{(R)})$$

$$\text{with } G_q = f_q^{\text{eq.}-} + \Phi_q + \frac{1}{2}p_q. \tag{49}$$

Note that the S_q and the G_q terms are equal to those in (40)–(41). The following elements of the interface collision operator have to be defined: $\lambda_e^{(I)}$ and $\{f_q^{\text{eq.}+(I)}\}$ (or at least $\{p_q^{(I)}\}$), $\{\lambda_q^{-(I)}\}$ and $\{f_q^{\text{eq.}-(I)}\}$ (or at least $\{m_q^{(I)}\}$), and the interface source term $\mathcal{Q}_q^{(I)}$.

4. HYDRODYNAMIC EQUATIONS: INTERFACE ANALYSIS

We analyze the interface conditions assuming that the equilibrium function is given by rel. (10) in the bulk, the source term is represented by the forcing (first rel. (2)), and the collision operator has two eigenvalue functions (8): $\Lambda_e^{(i)}$, proportional to the kinematic viscosity value $\nu^{(i)}$, and a free parameter $\Lambda_o^{(i)}$. For all numerical tests, the $d3Q15$ velocity set is used. We put "red" fluid below the interface and "blue" fluid above it.

4.1. Implicit Interface: Continuity Relations

We analyze rel. (40)–(41) derived for the implicit interface $\vec{\mathbf{r}}^{(I)}$ (see Fig. 1).

4.1.1. Pressure and tangential shear stress tensor

We first consider rel. (40) where, using rel. (36) with rel. (2),

$$m_q{}^{[2]} + \mathcal{Q}_q = \partial_q(-\Lambda_e p_q^{[1]}). \tag{50}$$

According to rel. (36), $p_q{}^{[2]} = O(\varepsilon^3)$ and rel. (40) becomes

$$[f_q^{\text{eq.}+(R)} - \Lambda_e^{(R)} p_q^{(R)}](\vec{\mathbf{r}}^{(I)}) = [f_{\bar{q}}^{\text{eq.}+(B)}(\vec{\mathbf{r}}^{(I)}) - \Lambda_e^{(B)} p_q^{(B)}](\vec{\mathbf{r}}^{(I)}) + O(\varepsilon^3), \tag{51}$$

$$\text{where } f_q^{\text{eq.}+}(\vec{\mathbf{r}}^{(I)}) = f_q^{\text{eq.}+}(\vec{\mathbf{r}}) + \frac{m_q{}^{[1]}}{2} = f_q^{\text{eq.}+} + \frac{\partial_q f_q^{\text{eq.}+}}{2},$$

$$\Lambda_e p_q(\vec{\mathbf{r}}^{(I)}) = \Lambda_e p_q(\vec{\mathbf{r}}) + \frac{1}{2}\partial_q(\Lambda_e p_q). \tag{52}$$

Let $q_\perp$ identify the *vertical links*. With the assumption that $\partial_z j_z(\vec{\mathbf{r}}^{(I)}) = 0$, then $p_{q_\perp}^{[1]} = 0$ and, therefore, $f_{q_\perp}^{\text{eq.}+(R)} = f_{q_\perp}^{\text{eq.}+(B)}$ in rel. (51). Provided that the equilibrium weights are continuous, the interface condition (51) reduces to the pressure

continuity condition (18)

$$P^{(R)}(\vec{\mathbf{r}}^{(I)}) = P^{(B)}(\vec{\mathbf{r}}^{(I)}), \quad \text{when } E^{(R)}_{q_\perp}(\vec{\mathbf{r}}^{(I)}) = E^{(B)}_{q_\perp}(\vec{\mathbf{r}}^{(I)}). \tag{53}$$

The last condition is valid, e.g., for Stokes equilibrium function ($E^{(u)}_q(\vec{\mathbf{u}}) = 0$ in rel. (10)), or when $j_z = 0$, or when $u_z(\vec{\mathbf{r}}^{(I)})$ is continuous and densities are equal, $\rho_0^{(R)} = \rho_0^{(B)}$. Including the surface tension term into $f_q^{\text{eq.}+}$ may modify the pressure continuity relation (see Ref. 19). We then multiply rel. (51) by $C_{q\alpha}$, $\alpha = \{x, y\}$ and take the sum over the interface links. The obtained relation,

$$\left[\Lambda_e^{(R)} \sum_{q\in I} p_q^{(R)} C_{q\alpha}\right](\vec{\mathbf{r}}^{(I)}) = \left[\Lambda_e^{(B)} \sum_{q\in I} p_q^{(B)} C_{q\alpha}\right](\vec{\mathbf{r}}^{(I)}) + O(\varepsilon^3) \tag{54}$$

states that the continuity for the tangential shear stress components $\nu\mathcal{D}_{\alpha z}$ in the form (17) since $\nu\mathcal{D}_{\alpha z} = \frac{2}{3}\Lambda_e \sum_{q\in I} p_q C_{q\alpha} + O(\varepsilon^3)$.

4.1.2. Momentum and velocity

The interface condition (41) is related to the continuity of the link momentum component j_q. We first neglect Φ_q from (41), as related to the pressure gradient and second derivatives of j_q. The remaining term, $f_q^{\text{eq.}-} + \frac{1}{2}\mathcal{Q}_q + \frac{1}{2}p_q{}^{[1]}$, with $p_q{}^{[1]} = \partial_q f_q^{\text{eq.}-}$, represents the first order Taylor expansion for j_q, then

$$j_q^{(R)}(\vec{\mathbf{r}}^{(I)}) = j_q^{(B)}(\vec{\mathbf{r}}^{(I)}) + O(\varepsilon^2), q \in I. \tag{55}$$

Taking a sum over the interface links which go through a given point $\vec{\mathbf{r}}^{(I)}$, one obtains the continuity condition for the normal component $j_z(\vec{\mathbf{r}}^{(I)})$. Substituting condition $j_z^{(R)} = j_z^{(B)}$ into rel. (55), one derives the continuity condition for the tangential momentum components. Then,

$$j_\alpha^{(R)}(\vec{\mathbf{r}}^{(I)}) = j_\alpha^{(B)}(\vec{\mathbf{r}}^{(I)}), \quad \alpha = \{x, y, z\}. \tag{56}$$

We emphasize that condition (56) is not equivalent to the continuity of the tangential velocity, Eq. (16), when two densities differ and $j_\alpha \neq 0$.

4.1.3. Simple Two-phase Flows

We consider two phase Stokes flows:

$$\begin{aligned} \mu^{(R)}\Delta\vec{\mathbf{u}} &= \nabla P^{(R)} - \vec{\mathbf{F}}^{(R)}, \quad z < z^{(I)}, \\ \mu^{(B)}\Delta\vec{\mathbf{u}} &= \nabla P^{(B)} - \vec{\mathbf{F}}^{(B)}, \quad z > z^{(I)}. \end{aligned} \tag{57}$$

We assume the Stokes equilibrium distribution unless indicated otherwise.

Linear flows. The continuity conditions, Eq. (56) for the momentum, Eq. (53) for pressure, and Eq. (54) for viscous stress tangential components are valid exactly

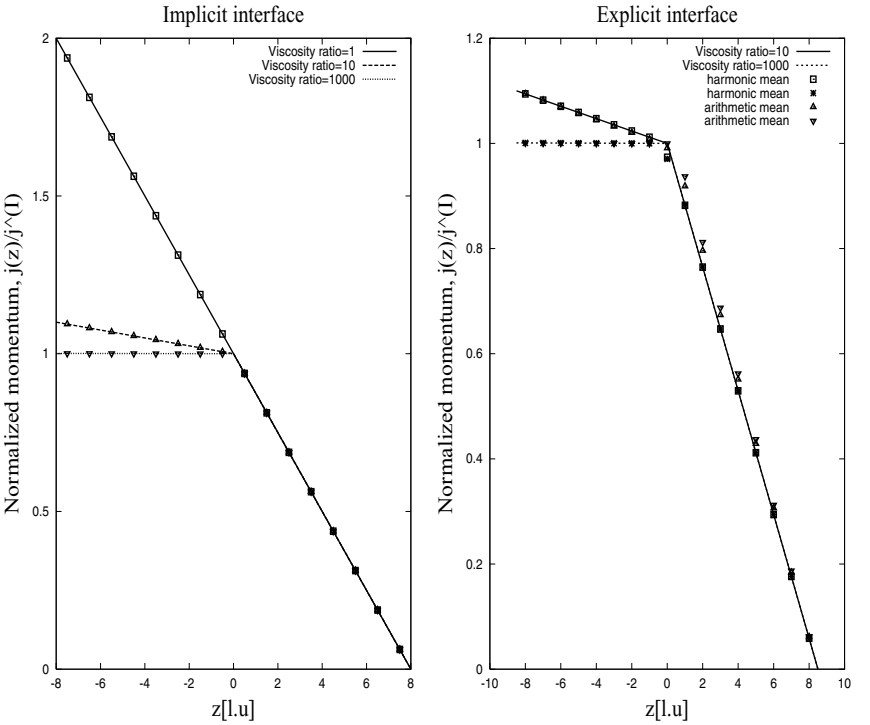

Fig. 3. Two phase Couette (shear) flow with the viscosity ratios $\nu^{(R)}/\nu^{(B)} = \Lambda_e^{(R)}/\Lambda_e^{(B)} = \{1, 10, 10^3\}$ is computed with the **implicit (left)** and **explicit (right)** interfaces located at the middle of the channel. Data: $\Lambda_e^{(R)} = 1$, $j_\alpha(-H) = 0.05(l.u)$, $j_\alpha(H) = 0$. **Implicit interface** (z=0): *solution is exact.* **Explicit interface** (z=0): *When $\nu^{(I)}$ is computed as a harmonic mean of $\nu^{(R)}$ and $\nu^{(B)}$, the solution is exact in the bulk.* The solution is inexact when $\nu^{(I)}$ is computed as an arithmetic mean, unless $\nu^{(R)} = \nu^{(B)}$.

midway along the link when $\Phi_q = 0$ and $p_q^{[2]} = 0$. The simplest flow which satisfies these conditions is two phase Couette (shear) flow parallel to solid boundaries ($\nabla P \equiv 0$, $\vec{\mathbf{F}} \equiv 0$). The bounce-back condition with the addition of a prescribed boundary momentum value maintains the linear momentum distributions exactly when solid boundaries are located midway between grid nodes and parallel to the main lattice axes. Linear boundary interpolations[2,22] maintain such solutions exactly for any arbitrary location of the walls with respect to the lattice. The free eigenvalue function Λ_o has no impact on the linear solutions. The picture on the left in Fig. 3 demonstrates that the obtained solution $j_\alpha(z)$ fits exactly the piece-wise linear distribution, regardless of the viscosity ratio, provided that the interface lies midway between two rows of grid nodes.

For Couette flow, the distribution $j_\alpha(z)$ is independent of the uniform pressure distribution $P(z)$. If, following,[41] one assumes two distinct fluid densities $\rho_0^{(i)} = P^{(i)}/c_s^{2(i)}$, and computes the tangential velocity as $u_\alpha^{(i)} = j_\alpha^{(i)}/\rho_0^{(i)}$, then, necessarily, the velocity $u_\alpha^{(i)}$ will undergo a jump on the interface, $u_\alpha^{(R)}/u_\alpha^{(B)} = \rho_0^{(B)}/\rho_0^{(R)}$ (even when the kinematic viscosities are equal) and the continuity condition (16) will be violated.

Parabolic flows. As a next example we consider two phase Poiseuille flow parallel to solid boundaries where the one dimensional parabolic velocity profile $u_\alpha^{(i)}(z)$, $\alpha = x$ or $\alpha = y$, satisfies the no-slip condition. The interface conditions are given by rel. (16), (18) where $u_z \equiv 0$. The LB solutions may match Poiseuille flows, e.g., with the piece-wise constant force values and no pressure gradients:

$$\mathcal{Q}_q^{-(i)} = \left[s_q^f t_q^\star(\vec{\mathbf{F}}\cdot\vec{\mathbf{C}}_q)\right]^{(i)}, \quad \sum_{q=1}^{Q-1} s_q^f t_q^\star C_{q\alpha}^2 = 1, \quad \text{then } F_\alpha^{(i)} = -\nu^{(i)}\partial_z^2 j_\alpha^{(i)}. \tag{58}$$

The obtained pressure distribution is then uniform and $m_q{}^{[1]} \equiv 0$. It follows from rel. (54), that the piece-wise linear distribution $\nu^{(i)}\partial_z j_\alpha^{(i)}(z)$ is continuous midway between grid rows. It follows from rel. (41), (55) that the parabolic distribution, $j_\alpha(z)$, is continuous midway along the link if, for *the diagonal interface links*

$$\begin{aligned}\Phi_q^{(R)} - \frac{1}{8}\partial_q^2 f_q^{eq.-(R)} &= \Phi_q^{(B)} - \frac{1}{8}\partial_q^2 f_q^{eq.-(B)}, \quad \text{where } \Phi_q = -\Lambda_o m_q{}^{[2]} \\ &= \Lambda_o(\Lambda_e\partial_q^2 f_q^{\text{eq.}-} + \mathcal{Q}_q^-), \quad C_{q\alpha}C_{qz} \neq 0. \end{aligned} \tag{59}$$

Substituting $\mathcal{Q}_q^{-(i)} = -[s_q^f \frac{\Lambda_e}{3}\partial_q^2 f_q^{\text{eq.}-}]^{(i)}$ into Eq. (59), and choosing equal values $s_q^{f(i)} = s^f$ for diagonal interface links, Eq. (59) is satisfied when

$$\Lambda_{eo} = [\Lambda_e\Lambda_o]^{(R)} = [\Lambda_e\Lambda_o]^{(B)} = \text{const}, \quad \text{if} \quad \frac{F^{(R)}}{\nu^{(R)}} = \frac{F^{(B)}}{\nu^{(B)}}, \tag{60}$$

$$\Lambda_{eo} = [\Lambda_e\Lambda_o]^{(R)} = [\Lambda_e\Lambda_o]^{(B)} = \frac{3}{8(3-s^f)}, \quad 0 \le s^f < 3, \quad \text{otherwise.} \tag{61}$$

Usually, we set $s_q^{f(i)} \equiv 1$. Then rel. (61) gives $\Lambda_{eo} = \frac{3}{16}$, i.e.:

$$\lambda_o^{(I)} = -8\frac{\lambda_e^{(i)} + 2}{\lambda_e^{(i)} + 8}. \tag{62}$$

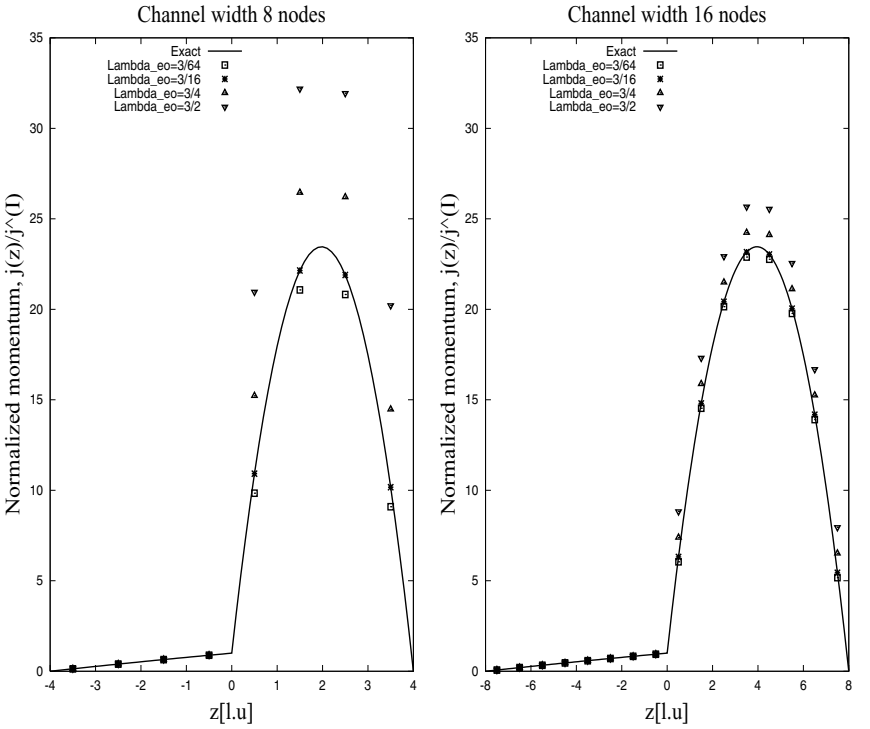

Fig. 4. Two phase Poiseuille flow with **implicit interface** and $\nu^{(R)}/\nu^{(B)} = 10^2$, $F^{(B)}/F^{(R)} = 10$ is computed using the bounce-back at solid boundaries and the different values for free parameter Λ_{eo}. Data: $\Lambda_e^{(R)} = 1$, $\Lambda_e^{(R)}\Lambda_o^{(R)} = \Lambda_e^{(B)}\Lambda_o^{(B)}$, $F^{(R)} = 5 \times 10^{-4}$ on the coarse grid (left) and $F^{(R)} = \frac{5}{4} \times 10^{-4}$ on the fine grid (right). *The solution is exact when* $\Lambda_{eo} = \frac{3}{16}$, $s^f = 1$, in agreement with rel. (61), (62)

The LB solution for Poiseuille flow therefore consists of two parabolic parts related by the following continuity conditions (using notation $||\psi|| = \psi^{(B)} - \psi^{(R)}$):

$$||\nu\partial_z j(z^{(I)})|| = 0, \quad ||T(j_\alpha)|| = 0, \quad \text{where}$$

$$T^{(i)}(j) = \left(j^{(i)} + \frac{1}{2}\partial_z j^{(i)} + \frac{(3 - s^f)}{3}[\Lambda_o \Lambda_e \partial_z^2 j]^{(i)} \right)(\vec{\mathbf{r}}^{(i)}). \qquad (63)$$

Remarkably, the closure relation corresponding to the bounce-back rule, applied at the boundary node $\vec{\mathbf{r}}_b$, is exactly $T(j_\alpha(\vec{\mathbf{r}}_b)) = 0$ (see Refs. 18, 22).

For single phase flow, an effective location of the no-slip wall at $z = H^{\text{eff}}$ is shifted from the assumed location $z = H$ (midway between grid nodes): $H^{\text{eff}2} - H^2 = \frac{4}{3}\Lambda_{eo} - \frac{1}{4}$ when $s_q^f \equiv 1$. Therefore the boundary error increases linearly with the viscosity when the free parameter Λ_o is fixed, unless condition (62) is satisfied. One should keep Λ_{eo} at a fixed value for the computations of the

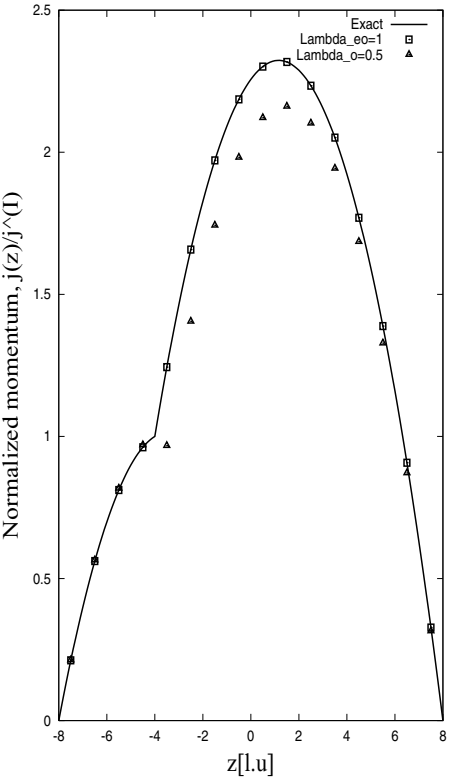

Fig. 5. Two phase Poiseuille flow with the equal curvatures, $F^{(R)}/\nu^{(R)} = F^{(B)}/\nu^{(B)}$, $\nu^{(R)}/\nu^{(B)} = \Lambda_e^{(R)}/\Lambda_e^{(B)} = 10$ and an **implicit interface** at $z = -4$. The solutions are computed with $\Lambda_{eo} = \Lambda_e^{(R)}\Lambda_o^{(R)} = \Lambda_e^{(B)}\Lambda_o^{(B)} = 1$ and with $\Lambda_o^{(R)} = \Lambda_o^{(B)} = \frac{1}{2}$. *Exact solution corresponds to equal* Λ_{eo} *values, in agreement with rel.* (60).

permeability of the porous media, otherwise the derived permeability values will depend on the fluid viscosity, via the condition $T(j_\alpha(\vec{\mathbf{r}}_b)) = 0$. Fixed Λ_{eo} values maintain viscosity independent permeabilities for any arbitrary porous media, because of the specific form of the coefficients in the closure relation imposed by the bounce-back condition (see Refs. 22, 44).

For two-phase flow, when conditions (60)–(61) are not satisfied, the second order error combines two components, the boundary error of the bounce-back condition and the interface error of the implicit coupling. Figure 4 demonstrates the impact of the free eigenvalue combination $\Lambda_{eo} = \Lambda_e^{(R)}\Lambda_o^{(R)} = \Lambda_e^{(B)}\Lambda_o^{(B)}$ on the obtained solutions. All numerical computations are done with $s_q^f = 1$. The exact solution is obtained with $\Lambda_{eo}^{(i)} = \frac{3}{16}$ what is in agreement with the analysis. The normalized error $(j(z) - j^{\text{th}}(z))/j^{(I)}$ is higher here for the less viscous phase.

We then separate the boundary and the interface errors, performing the boundary conditions exactly with the help of the third order accurate multi-reflection condition MRI (see Table 2 in Ref. 22). Figure 5 addresses the case of equal curvature. In agreement with rel. (60), the solution is exact for any equal combinations $\Lambda_{eo}^{(i)}$. Taking equal free eigenvalue functions, here $\Lambda_o^{(R)} = \Lambda_o^{(B)} = \frac{1}{2}$, the solution deviates from the exact profile when $\nu^{(R)} \neq \nu^{(B)}$ and, therefore, $\Lambda_{eo}^{(R)} \neq \Lambda_{eo}^{(B)}$.

Solution (61) is also valid when the constant pressure gradient and the constant forcing are combined, or when the force is absent and $m_q{}^{[1]}$ replaces $-\mathcal{Q}_q^-$ in rel. (59) (for diagonal interface links, $m_q^{[1]} = t_q^\star(\nabla P \cdot \vec{\mathbf{C}}_q) = \frac{\Lambda_e}{3}\partial_q^2 f_q^{\text{eq.}-}$). The solution (62) was first obtained for the two phase FCHC MRT model in Ref. 17. TRT and MRT models based on the cubic velocity sets will obtain equal parabolic distributions when the even eigenvalues, related to kinematic viscosity, and the odd eigenvalues, associated to the third order polynomial basis vectors $C_{q\alpha}(C_{qz}^2 - \text{const})$, satisfy rel. (60)–(61). The other even MRT eigenvalues do not influence the Poiseuille flow solutions unless the Navier-Stokes equilibrium function is used. When the non-linear term is included, the solution $j_\alpha^{(i)}(z)$ does not alter, using the "compressible" or "incompressible"equilibrium forms, for any values of other even eigenvalues. On the contrary, for the TRT-operator only, the solution $\rho(z)$, and therefore $j_\alpha^{(i)}(z)/\rho(z)$ is not modified (for MRT model, see rel. A.13-A.15 in Ref. 21).

When the interface is not parallel to the coordinate axes, all first order results remain valid, due to rotational invariance of the first order expansion, but not solution (61), because of the lack of invariance for the second order terms. Particular solutions for $\lambda_o(\lambda_e)$ are derived in Refs. 17, 19 for inclined channels.

When the obtained pressure distribution is uniform or linear, the solution for $j_\alpha(z)$ does not depend on the employed values of $c_s^{2(i)}$ and $\rho_0^{(i)}$, and the solution for $u_\alpha^{(i)} = j_\alpha^{(i)}/\rho_0^{(i)}$ is therefore discontinuous on the interface when two densities differ, like for the case of Couette flow.

4.2. Explicit Interface: Collision Components

We now analyze rel. (48)–(49) derived for the explicit interface $\vec{\mathbf{r}}^{(I)}$ (see Fig. 2).

4.2.1. Pressure and Tangential Shear Stress Components

Let us consider first Eq. (48). For forcing (2), $\mathcal{Q}_q^{(I)} - \mathcal{Q}_{\bar{q}}^{(I)} = 2\mathcal{Q}_q^{(I)}$, $-\mathcal{Q}_{\bar{q}}^{(R)} = \mathcal{Q}_q^{(R)}$. If we set

$$\mathcal{Q}_q^{(I)} = \frac{1}{2}\left(\mathcal{Q}_q^{(R)} + \mathcal{Q}_q^{(B)}\right), \tag{64}$$

then the forcing terms vanish in rel. (48). If we set then

$$m_q^{(I)} = \frac{1}{2}\left(m_q^{(R)} + m_q^{(B)}\right), \tag{65}$$

the odd order terms vanish in rel. (48) and we obtain for $\vec{\mathbf{r}} = \vec{\mathbf{r}}^{(I)}$:

$$\left[f_q^{\text{eq.}+(R)} - \Lambda_e^{(R)} p_q^{(R)}\right] = \left[f_q^{\text{eq.}+(B)} - \Lambda_e^{(B)} p_q^{(B)}\right]. \tag{66}$$

This condition is equivalent to rel. (51) and further analysis is identical. The continuity for pressure and tangential stress tensor components can then be established for the interface node $\vec{\mathbf{r}}^{(I)}$ under the conditions (37), (53) and provided that the interface quantity $m_q^{(I)}$ is defined via rel. (65). Choosing equal free eigenvalues, $\lambda_o^{(I)} = \lambda_o^{(R)} = \lambda_o^{(B)}$, rel. (65) becomes

$$f_q^{\text{ne.}-(I)} = \frac{1}{2}\left(f_q^{\text{ne.}-(R)} + f_q^{\text{ne.}-(B)}\right), \tag{67}$$

or, replacing $f_q^{\text{ne.}-(I)}$ by its definition (see Eq. (47)) and taking into account that $f_q^{\text{eq.}+(R)} = f_q^{\text{eq.}+(B)}$ owing continuity of the pressure, we get:

$$f_q^{\text{eq.}-(I)} = \frac{1}{2}\left(f_q^{\text{eq.}-(R)} + f_q^{\text{eq.}-(B)}\right) + \frac{1}{2}\left(f_q^{\text{ne.}+(R)} - f_q^{\text{ne.}+(B)}\right). \tag{68}$$

This means that the interface equilibrium anti-symmetric part should differ from its continuation in the bulk when the $f_q^{\text{eq.}-(R)}(\vec{\mathbf{r}}^{(I)}) = f_q^{\text{eq.}-(B)}(\vec{\mathbf{r}}^{(I)})$, i.e. when momentum is continuous, unless two viscosities are equal ($f_q^{\text{ne.}+(R)} = f_q^{\text{ne.}+(B)}$). This property is further analyzed in Sec. 4.2.3.

4.2.2. Interface Viscosity

Let us consider now Eq. (49). For forcing (2), $\mathcal{Q}_q^{(I)} + \mathcal{Q}_{\bar{q}}^{(I)} = 0$. We define first $f_q^{\text{eq.}+(I)}$:

$$f_q^{\text{eq.}+(I)} = \frac{1}{2}\left(f_q^{\text{eq.}+(R)} + f_{\bar{q}}^{\text{eq.}+(R)}\right). \tag{69}$$

Using this definition, we split $f_q^{\text{ne.}+(I)}$ into two parts:

$$\begin{aligned} f_q^{\text{ne.}+(I)} &= f_q^{\text{ne.}+(I)[1]} + f_q^{\text{ne.}+(I)[2]}, \\ f_q^{\text{ne.}+(I)[1]} &= \frac{1}{2}(f_q^{\text{ne.}+(R)} + f_q^{\text{ne.}+(B)}), \\ f_q^{\text{ne.}+(I)[2]} &= \frac{1}{2}(f_q^{-(R)} - f_q^{-(B)}). \end{aligned} \tag{70}$$

If we set in Eq. (49)

$$\begin{cases} \lambda_e^{(I)}(\frac{p_q^{(R)}}{\lambda_e^{(R)}} + \frac{p_q^{(B)}}{\lambda_e^{(B)}}) & = p_q^{(R)} + p_q^{(B)}, \\ \frac{\lambda_e^{(I)}}{2}(f_q^{-(R)} - f_q^{-(B)}) & = \Phi_q^{(B)} - \Phi_q^{(R)}, \end{cases} \tag{71}$$

then Eq. (49) becomes

$$[2f_q^{\text{eq.}-(R)} + \mathcal{Q}_q^{(R)}](\vec{\mathbf{r}}^{(I)}) = [2f_q^{\text{eq.}-(B)} + \mathcal{Q}_q^{(B)}](\vec{\mathbf{r}}^{(I)}). \tag{72}$$

This condition is equivalent to the continuity condition (55) for the momentum components $j_q^{(i)}$. Further analysis of this relation yields the continuity of the normal and tangential momentum components.

One can try to derive the solution for $\lambda_e^{(I)}$ from Eq. (71). Multiplying the first line in rel. (71) by $C_{q\alpha}$, and taking their sum, they become:

$$\lambda_e^{(I)}(\frac{\mathcal{D}_{\alpha z}^{(R)}}{\lambda_e^{(R)}} + \frac{\mathcal{D}_{\alpha z}^{(B)}}{\lambda_e^{(B)}}) = \mathcal{D}_{\alpha z}^{(R)} + \mathcal{D}_{\alpha z}^{(B)}, \tag{73}$$

or, equivalently,

$$\Lambda_e^{(I)} = \frac{\Lambda_e^{(B)} r_v + \Lambda_e^{(R)}}{r_v + 1}, \quad r_v = \frac{\mathcal{D}_{\alpha z}^{(B)}}{\mathcal{D}_{\alpha z}^{(R)}}. \tag{74}$$

It follows from the continuity of the tangential stress components that

$$r_v = \frac{\nu^{(R)}}{\nu^{(B)}} = \frac{\Lambda_e^{(R)}}{\Lambda_e^{(B)}}. \tag{75}$$

Substituting this relation into rel. (74), the interface viscosity value, $\nu^{(I)} = \frac{1}{3}\Lambda_e^{(I)}$, becomes equal to the *harmonic mean value* of $\nu^{(R)}$ and $\nu^{(B)}$:

$$\nu^{(I)} = \frac{2\nu^{(R)}\nu^{(B)}}{\nu^{(R)} + \nu^{(B)}}. \tag{76}$$

Let us comment on this solution. Grunau[30] constructs a parabolic approximation which links two relaxation parameters $\tau^{(i)} = -\frac{1}{\lambda_e^{(i)}}$ and leads to the harmonic mean value for the *interface averaged parameter* $\tau^{(I)} = 2\tau^{(R)}\tau^{(B)}/(\tau^{(R)} + \tau^{(R)})$, or, equivalently, the arithmetic mean value for the interface eigenvalue $\lambda_e^{(I)}$. This solution differs from (76). Most often, $\nu^{(I)}$ is computed with the linear interpolations where the weights are related to the phase indicator value (e.g., the mass fractions in Ref. 54 or the index function in Ref. 31). The estimation error of the surface tension coefficient, created via the perturbation term, reduces when the interface viscosity is computed by the weighted mean value (see in Ref. 20). The current analysis shows that the exact transport of the non-equilibrium components, corresponding to the interface condition (17), can be achieved with the

harmonic mean value of the kinematic bulk viscosities. Note that this condition is not equivalent to the harmonic mean value of the dynamic bulk viscosities when the two densities differ.

4.2.3. Free Collision Parameters

Taking into account the continuity condition (72), it arises that

$$f_q^{-(R)} - f_q^{-(B)} = \left(\frac{m_q^{(R)}}{\lambda_o^{(R)}} - \frac{m_q^{(B)}}{\lambda_o^{(B)}} \right) - \frac{1}{2} \left(\mathcal{Q}_q^{-(R)} - \mathcal{Q}_q^{-(B)} \right). \tag{77}$$

We substitute this relation into the second line of rel. (71), which reads

$$\frac{1}{2} \lambda_e^{(I)} (f_q^{-(R)} - f_q^{-(B)}) = \Lambda_o^{(R)} m_q^{(R)} - \Lambda_o^{(B)} m_q^{(B)}. \tag{78}$$

When $\lambda_o^{(R)} = \lambda_o^{(B)} = \lambda_o^{(I)}$ and parabolic flows are considered, where for diagonal interface links $\mathcal{Q}_q^{-(i)} = -s^f [\frac{\Lambda_\epsilon}{3} \partial_q^2 f_q^{\text{eq.}-}]^{(i)}$ and $\partial_q P^{(R)} = \partial_q P^{(B)}$, we obtain

$$\frac{m_q^{(R)} - m_q^{(B)}}{\mathcal{Q}_q^{-(R)} - \mathcal{Q}_q^{-(B)}} = \frac{3 - s^f}{s^f}, \quad 0 \le s^f < 3, \quad \text{if} \quad \mathcal{Q}_q^{-(R)} \neq \mathcal{Q}_q^{-(B)}, C_{q\alpha} C_{qz} \neq 0. \tag{79}$$

From Eq. (78) with rel. (77), (79) the solution for $\Lambda_o^{(I)}$ is

$$\Lambda_o^{(I)} = \Lambda_o^{(R)} = \Lambda_o^{(B)}, \quad \text{if} \quad F^{(R)} = F^{(B)},$$
$$\Lambda_{eo}^{(I)} = \Lambda_o^{(I)} \Lambda_e^{(I)} = \frac{3}{4(3 - s^f)}, \quad \Lambda_o^{(I)} = \Lambda_o^{(R)} = \Lambda_o^{(B)}, \quad \text{if} \quad F^{(R)} \neq F^{(B)}. \tag{80}$$

Solution (80) differs by a factor 2 from solution (61), obtained for the implicit interface.

4.2.4. Summary

The first order analysis shows that the immobile interface node $\vec{\mathbf{r}}^{(I)}$ will maintain continuity of the symmetric equilibrium part, $f_q^{\text{eq.}+(R)} = f_q^{\text{eq.}+(B)}$, momentum, $\vec{j}^{(R)} = \vec{j}^{(B)}$, and tangential shear stress, $\nu^{(R)} \mathcal{D}_{\alpha z}^{(R)} = \nu^{(B)} \mathcal{D}_{\alpha z}^{(B)}, \alpha = \{x, y\}$, provided that the interface collision components satisfy, for the interface links, the conditions (64), (65), (69) and when the interface viscosity is given by rel. (76). These conditions are

$$\mathcal{Q}_q^{(I)} = \frac{1}{2} (\mathcal{Q}_q^{(R)} + \mathcal{Q}_q^{(B)}). \tag{81}$$

$$m_q^{(I)} = \frac{1}{2}(m_q^{(R)} + m_q^{(B)}), \tag{82}$$

$$f_q^{\text{eq.}+(I)} = \frac{1}{2}(f_q^{\text{eq.}+(R)} + f_q^{\text{eq.}+(B)}), \tag{83}$$

$$\nu^{(I)} = \frac{2\nu^{(R)}\nu^{(B)}}{\nu^{(R)} + \nu^{(B)}}. \tag{84}$$

Let us illustrate them for the piece-wise linear, two phase flow in the absence of force ($\vec{\mathbf{j}} = \vec{\mathbf{J}}$). The arriving exact solution is

$$f_q^{(I)} = f_q^{\text{eq.}(R)} + \frac{t_q^\star}{\lambda_e^{(R)}}\nabla_q j_q^{(R)}, \quad f_{\bar{q}}^{(I)} = f_{\bar{q}}^{\text{eq.}(B)} + \frac{t_q^\star}{\lambda_e^{(B)}}\nabla_q j_q^{(B)},$$
$$m_q^{(R)} = m_q^{(B)} = 0, \quad q \in I. \tag{85}$$

If $m_q^{(I)} = 0$ according to rel. (82), then the populations leaving the interface maintain exactly solution (85), due to choice of the interface viscosity (84) (see rel. (73)):

$$\tilde{f}_q^{(I)} = f_q^{\text{eq.}(B)} + t_q^\star\left(\frac{1}{\lambda_e^{(B)}} + 1\right)\nabla_q j_q^{(B)},$$
$$\tilde{f}_{\bar{q}}^{(I)} = f_{\bar{q}}^{\text{eq.}(R)} + t_q^\star\left(\frac{1}{\lambda_e^{(R)}} + 1\right)\nabla_{\bar{q}} j_{\bar{q}}^{(R)}, \quad q \in I. \tag{86}$$

However, Eq. (82) yields rel. (68), which gives here exactly:

$$j_q^{(I)} = \frac{1}{2}(j_q^{(R)} + j_q^{(B)})(\vec{\mathbf{r}}^{(I)}) + \delta j_\alpha C_{q\alpha}, \quad q \in I$$
$$\delta j_\alpha = \frac{1}{2}\left(\frac{\partial_z j_\alpha^{(R)}}{\lambda_o^{(R)}} - \frac{\partial_z j_\alpha^{(B)}}{\lambda_o^{(B)}}\right) = \frac{1}{4}\left(\partial_z j_\alpha^{(B)} - \partial_z j_\alpha^{(R)}\right), \quad \alpha = \{x, y\}. \tag{87}$$

Therefore, when

$$j_\alpha^{(I)} = \frac{1}{2}(j_\alpha^{(R)} + j_\alpha^{(B)})(\vec{\mathbf{r}}^{(I)}) + \delta j_\alpha, \quad \alpha = 1, \ldots, d, \tag{88}$$

then the piece-wise linear solution is exact in the bulk, and vice-versa. However, when the arriving populations bring continuous values, the total momentum $j_\alpha^{(I)}$ will differ by the quantity δj_α. The deficiency δj_α is due to the difference between the kinematic viscosities and it converges linearly with space refinement.

Linear flow. Let us illustrate the obtained relations using two phase Couette flow where $m_q^{(R)} = m_q^{(B)} = 0$ and $\lambda_o^{(i)}$ may take arbitrary values, in agreement with rel. (78). We set $f_q^{\text{eq.}-}(\vec{\mathbf{r}}^{(I)}) = t_q^\star(\vec{\mathbf{j}}^{(I)} \cdot \vec{\mathbf{C}}_q)$, $\vec{\mathbf{j}}^{(I)} = \vec{\mathbf{J}}^{(I)}$, $\vec{\mathbf{J}}^{(I)}$ being the total population momentum. The picture on the right in Fig. 3 shows the obtained

solutions. The distribution $j_\alpha(z)$ is exact in the bulk and satisfies rel. (87) on the interface, when $\nu^{(I)}$ is computed by the harmonic mean value. The picture also shows the piece-wise linear solutions obtained with the arithmetic mean value, $\nu^{(I)} = (\nu^{(R)} + \nu^{(B)})/2$. The obtained shear ratio is then correct but the solution is inexact since the interface viscosity does not maintain the exact transfer of the non-equilibrium parts. The total interface momentum does not correspond to a continuation of the bulk values, but the discrepancy is smaller than those obtained with the harmonic mean values.

Parabolic flow. When the force is present, one should replace $\vec{\mathbf{j}}^{(i)}$ with $\vec{\mathbf{J}}^{(i)}$ in rel. (87). Solution (88) is valid however for both, $\vec{\mathbf{j}}^{(i)} = \vec{\mathbf{J}}^{(i)} + \frac{1}{2}\vec{\mathbf{F}}^{(i)}$ and $\vec{\mathbf{J}}^{(i)}$, due to rel. (81) for the interface forcing. When the forces are equal, the exact Poiseuille solution requires that free eigenvalues are equal, $\lambda_o^{(R)} = \lambda_o^{(B)} = \lambda_o^{(I)}$, in addition to rel. (81)–(84). The bounce-back reflection will not maintain the exact solutions when the two viscosities differ since one cannot satisfy condition (61), $\Lambda_{eo}^{(i)} = \frac{3}{16}$, for both phases together. We use again MR1 boundary condition. Figure 6 confirms that, for the harmonic mean interface viscosity, the solution is exact in the bulk and its deviation on the interface corresponds to rel. (87), as with Couette flow. The solutions obtained with the arithmetic mean value consist of two parabolic profiles with correct curvature but lack the exact coupling of the tangential stress components.

When the forces differ, the eigenvalue combination $\Lambda_o^{(I)}\Lambda_e^{(I)}$ should be set equal to $\frac{3}{8}$ and both $\lambda_o^{(R)}$ and $\lambda_o^{(B)}$ values are set equal to $\lambda_o^{(I)}$ (see rel. (80)). Since this solution differs from the solution (61), $\Lambda_{eo}^{(i)} = \frac{3}{16}$, the bounce-back reflection will not maintain exact solutions, even when the two viscosities are equal. The picture on the left in Fig. 7 demonstrates the exact bulk solutions obtained for $\nu^{(R)}/\nu^{(B)} = 10^3$, $F^{(R)}/F^{(B)} = 10$, using the MR1 boundary conditions. The channel is discretized with 9 and 27 points, reducing forcing by a factor 3^2 for the finer grid. The obtained solutions satisfy rel. (87) on the interface and therefore, condition (82) is valid again. The interface correction δj_α converges linearly with space refinement.

When the pressure distribution is constant but bulk densities differ, it follows from condition (83) that $c_s^{2(I)} = \frac{1}{2}(c_s^{2(R)}\rho^{(R)}/\rho^{(I)} + c_s^{2(B)}\rho^{(B)}/\rho^{(I)})$, i.e. $c_s^{2(I)}$ is represented via a mass weighted combination when $\rho^{(I)} = (\rho^{(R)} + \rho^{(B)})/2$. The numerical simulations confirm that the solution does not change for $j_\alpha^{(i)}$ and therefore, $j_\alpha^{(i)}/\rho_0^{(i)}$ is again discontinuous on the interface when the two densities differ.

In conclusion we mention that the macroscopic interface quantities correspond mostly to a sum of the two separate moments in the two phase LB schemes. The equilibrium interface momentum value is adjusted artificially for some algorithms, e.g. in Ref. 43, when two separate evolution equations with BGK collisions are employed (see also the remark after Eq. (9)). The solution (88) and examples

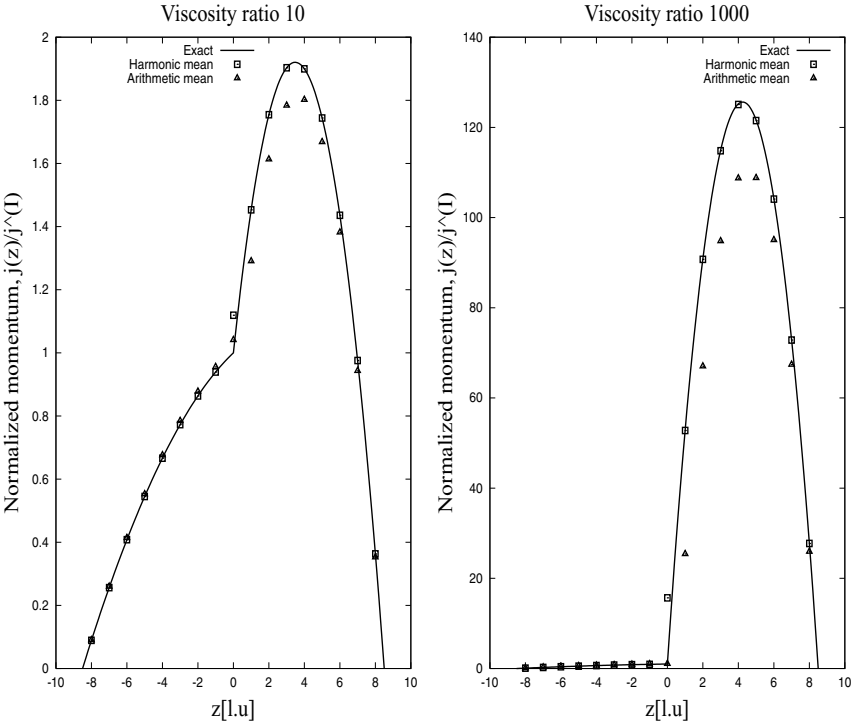

Fig. 6. Poiseuille two phase solutions with $\nu^{(R)}/\nu^{(B)} = 10$ (**left picture**) and $\nu^{(R)}/\nu^{(B)} = 10^3$ (**right picture**) and equal forcing are computed when the interface is located at the grid node $z = 0$. Interface kinematic viscosity is computed as a harmonic mean value and as an arithmetic mean value of bulk values. *The solution is exact for the harmonic mean value except for the interface node*, where its discrepancy agrees with rel. (87), (88). Data: $\Lambda_e^{(R)} = 1$, $F^{(R)} = F^{(B)} = 2.5 \times 10^{-4}(l.u)$.

above show that the method may give an exact bulk solution when the equilibrium momentum value differs from a continuation of the bulk values, naturally seen as a "physical" momentum value. Extrapolations from the bulk values can be employed to define the effective macroscopic solution for the interface nodes.

5. AADE: INTERFACE ANALYSIS

Assuming the generic equilibrium function (3) for the AADE, with the solution (21)–(24) for the combination $\mathcal{T}_q = \Lambda_q E_q$, we analyze the interface conditions assuming that the source term represents the mass source (rel. (2)) and the eigenvalues obey rel. (8). For all computations, the $d3Q15$ velocity set is used. We put "red" soil on the bottom and "blue" soil on top of the aquifer.

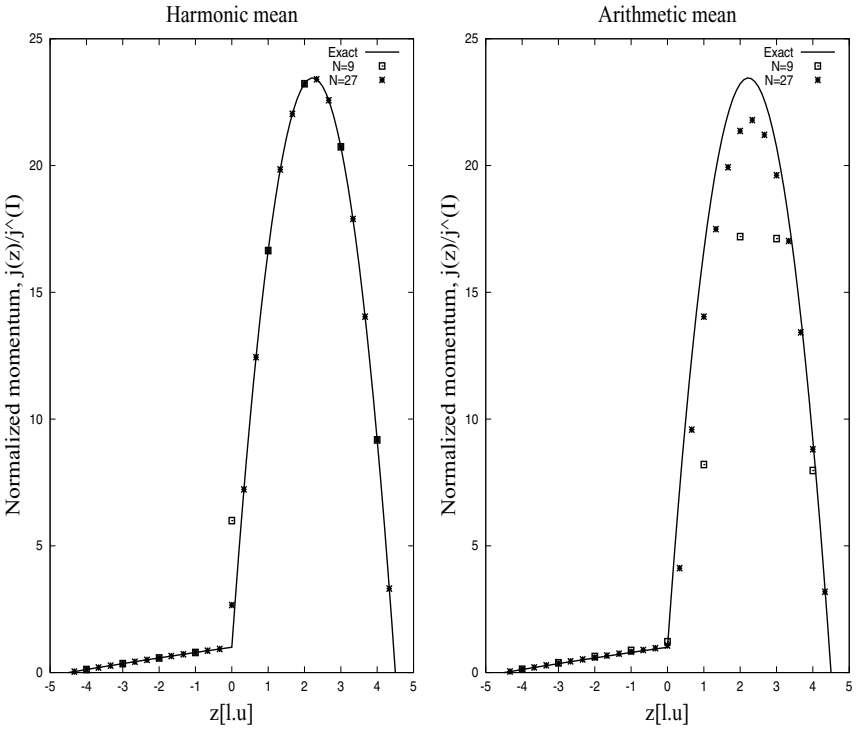

Fig. 7. Poiseuille two phase solutions with $\nu^{(R)}/\nu^{(B)} = 10^4$, $F^{(B)}/F^{(R)} = 10$, are computed when the explicit interface is located in the middle of the channel consisting from 9 and 27 nodes. Data: $\Lambda_e^{(R)} = 1$, $F^{(R)} = 5 \times 10^{-4}$ on the coarse grid. **Left picture**: $\nu^{(I)}$ is computed as a harmonic mean value of bulk values. *Solution is exact except for the interface node* $z = 0$ where it agrees with rel. (87), (88). **Right picture**: $\nu^{(I)}$ is computed as an arithmetic mean value.

5.1. Implicit Interface

We analyze rel. (40)–(41) derived for the implicit interface $z = z^{(I)}$, midway between the nodes with the "red" and "blue" collisions (see Fig. 1).

5.1.1. Advective-diffusive flux

The interface condition (41) is related to the continuity of the flux projection $f_q^{\text{eq.}-} + \Phi_q$. The term $\frac{1}{2}(p_q + \mathcal{Q}_q)$ represents a linear interpolation to point midway along the link: $\frac{1}{2}(p_q^{[1]} + p_q^{[2]} + \mathcal{Q}_q^{+}) = \frac{1}{2}(\partial_q f_q^{\text{eq.}-} + \partial_q \Phi_q)$ such that Eq. (41) becomes:

$$[f_q^{\text{eq.}-(R)} + \Phi_q^{(R)}](\vec{\mathbf{r}}^{(I)}) = [f_q^{\text{eq.}-(B)} + \Phi_q^{(B)}](\vec{\mathbf{r}}^{(I)}) + O(\varepsilon^3). \tag{89}$$

This continuity relation is exact when the flux components are linear functions of the coordinates. The sum of rel. (89) over all links going through $\vec{\mathbf{r}}^{(I)}$ corresponds to the normal flux continuity condition (33). We emphasize that the implicit interface conditions constrain not only the normal but also the tangential flux components. This may become incompatible with the continuity of the tangential derivatives on the soil boundaries in heterogeneous soils. This problem is addressed in Ref. 27.

5.1.2. Diffusion Variable

When the term $-\Lambda_e p_q + \mathcal{Q}_q$ is neglected, the interface condition (40) yields

$$f_q^{\text{eq.}+(R)}(\vec{\mathbf{r}}^{(I)}) = f_{\bar{q}}^{\text{eq.}+(B)}(\vec{\mathbf{r}}^{(I)}) + O(\varepsilon^2), \quad q \in I. \tag{90}$$

In particular, ${p_q}^{[1]} = {p_q}^{[2]} = 0$ when the advective-diffusive flux is constant. For the equilibrium function (3) with $f_q^{\text{eq.}+(i)} = E_q^{(i)} h'^{(i)}$, the diffusive variable $h'(\vec{\mathbf{r}}^{(I)})$ is continuous when, necessarily,

$$\sum_{q \in I} E_q^{(R)}(\vec{\mathbf{r}}^{(I)}) = \sum_{\bar{q} \in \bar{I}} E_{\bar{q}}^{(B)}(\vec{\mathbf{r}}^{(I)}). \tag{91}$$

Equality of the weights, $E_q^{(R)} = E_{\bar{q}}^{(B)}$ presents a sufficient but not a necessary condition for the TRT-E model (see TRT-E description after rel. (24)). Continuity of the diffusion variable may disagree with the physical continuity condition. As an example, let us consider Richards' Equation (31) in isotropic heterogeneous media. Using the moisture content or the Kirchoff transform formulations, the continuity conditions (90) will induce the continuity of the water content variable $\theta(\vec{\mathbf{r}}^{(I)})$ or the one for the Kirchoff transform variable $\int_{-\infty}^{h'(\theta)} K'(h)dh$, respectively. When the retention curves $h(\theta)$ or the conductivities $K(h)$ differ for the two soils, the obtained pressure distribution should undergo a jump on the interface. Numerical computations confirm this analysis. We demonstrate in Sec. 5.1.4 that a mixed formulation, where the diffusion variable is proportional to the pressure head variable, matches correctly for transient solutions with sharp pressure gradients on the interfaces.

5.1.3. Simple Layered Solutions

Test solutions presented in this section can be obtained by either solving the diffusion equation ($h' = s$, s is a conserved quantity) directly, or by solving Richard's Eq. (31) in the saturated zone. In all simulations in this section, we use the pressure formulation to the steady state Richard's Eq. (31), with $\bar{\mathcal{D}}^{(i)}(s) = h'^{(i)}/H^{\text{eq.}}$ ($H^{\text{eq.}}$ as an accelerating parameter) and the diffusion tensor $\mathbf{K}'$.

Linear solutions. The advective-diffusive flux and the diffusion variable are both continuous exactly midway along the interface link when $p_q = 0$, $m_q^{[2]} = 0$

and $\mathcal{Q}_q = 0$. The simplest problem which satisfies these conditions is the vertical saturated flow in stratified aquifers, solution to Eq. (30). When the vertical axis is a principal axis of the permeability tensor, then the off-diagonal elements $K_{xz}^{'(i)}$ and $K_{yz}^{'(i)}$ vanish. The vertical flow corresponds to a piece-wise linear, continuous distribution $h(z)$ where $\partial_z h^{(i)}(z^{(I)})$ obeys the continuity condition (33). The simplest boundary condition to prescribe the Dirichlet condition midway between grid nodes, $f_q^{\text{eq.}+}(\vec{\mathbf{r}}_\text{b} + \frac{1}{2}\vec{\mathbf{C}}_q) = f_q^{\text{eq.}+(b)}$, is the anti-bounce-back rule, analyzed in Ref. 24:

$$f_{\bar{q}}(\vec{\mathbf{r}}_\text{b}, t+1) = -\tilde{f}_q(\vec{\mathbf{r}}_\text{b}, t) + 2 f_q^{\text{eq.}+(b)}. \tag{92}$$

The anti-bounce-back rule is exact when the distribution $\bar{\mathcal{D}}(\vec{\mathbf{r}})$ is piece-wise linear. With the purpose to find solutions for free parameters in rel. (21)–(24) which maintain the vertical flow exactly, we write down the exact population solution for both interface sides: $[f_q^{\text{eq.}+}(z)]^{(i)} = E_q^{(i)} h^{(i)}(z)$, $m_q{}^{(i)} \equiv E_q^{(i)} \partial_z h^{(i)} C_{qz}$, $p_q{}^{(i)} \equiv 0$. When the advection term is absent, the solution is maintained for each separate interface link *without any additional coupling terms*, if

$$E_q^{(R)} = E_q^{(B)}, \quad E_q^{(R)} \Lambda_q^{(R)} \partial_z \bar{\mathcal{D}}^{(R)} = E_q^{(B)} \Lambda_q^{(B)} \partial_z \bar{\mathcal{D}}^{(B)}, \quad \text{i.}e. \ \frac{\Lambda_q^{(R)}}{\Lambda_q^{(B)}} = r_z, \quad q \in I,$$

$$r_\alpha = [\partial_\alpha \bar{\mathcal{D}}^{(B)} / \partial_\alpha \bar{\mathcal{D}}^{(R)}](\vec{\mathbf{r}}^{(I)}), \quad r_z = \frac{K_{zz}^{'(R)}}{K_{zz}^{'(B)}} \ \text{ when } \ \vec{\mathbf{J}} = 0. \tag{93}$$

Let us consider how these conditions are handled by the L- and TRT-E collision strategies.

L-Model (isotropic weights, anisotropic eigenvalues): operating with the continuous positive weights, $E_q^{(i)} = c_e t_q^\star$, the model can try to satisfy the condition $\Lambda_q^{(R)} / \Lambda_q^{(B)} = r_z$ with a proper choice of two anisotropic sets of the eigenvalue functions. The following solution for $s_d^{(i)}$ is referred to below as *the vertical strategy* (available only if $S_z^{max} < D_z^{min}$):

$$\begin{aligned}
&s_d^{(i)} = \beta_v K_{zz}^{'(i)}, \quad \beta_v = (1 - 2t_1^\star) D_z^{min} + 2t_1^\star S_z^{max}, \\
&D_z^{min} = \min_i \left\{ \frac{D^{min(i)}}{K_{zz}^{'(i)}} \right\}, \quad D^{min(i)} = \min_{\alpha=1,\ldots,d} \{K_{\alpha\alpha}^{'(i)}\}, \quad S_z^{max} = \max_i \left\{ \frac{S^{max(i)}}{K_{zz}^{'(i)}} \right\}, \\
&S^{max(i)} = \max_q S_q^{(i)}, \quad S_q^{(i)} = \sum_{\alpha \neq \beta} K_{\alpha\beta}^{'(i)} C_{q\alpha} C_{q\beta}.
\end{aligned} \tag{94}$$

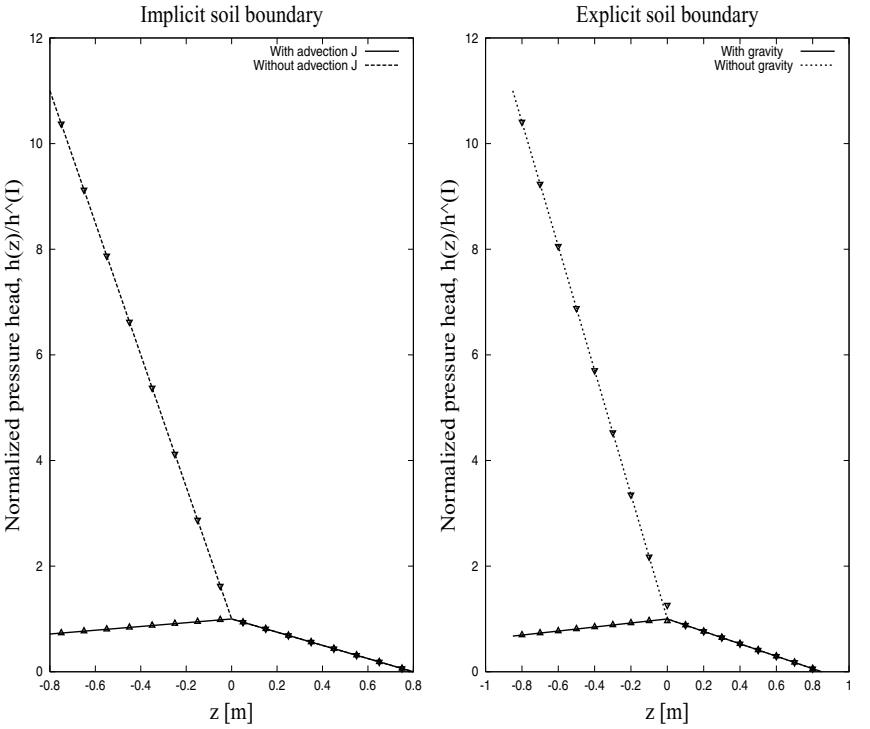

Fig. 8. Vertical flow is computed with the **implicit tracking (left)** and the **explicit tracking (right)** for the horizontal soil boundary, located at the middle of the heterogeneous aquifer. The permeability tensor is heterogeneous, $K_{zz}^{a(R)}/K_{zz}^{a(B)} = 1/10$, $K_s^{(R)} = K_s^{(B)} = \frac{1}{6}\ m^2/h$. Boundary conditions are: $h = 0.5\ m$ on the bottom and $h = 0$ on the surface. Scalings are: $\mathcal{U} = 1$ and $\mathcal{L} = 10$. The vertical eigenvalue strategies (94), (95) are used: e.g., in isotropic case: $\Lambda_o^{(R)} = \frac{1}{2}$, $\Lambda_o^{(B)} = 5$.

When the free parameter $s_d^{(i)}$ in (21)–(24) is computed with rel. (94), condition $\Lambda_q^{(R)}/\Lambda_q^{(B)} = D_{zz}^{(R)}/D_{zz}^{(B)}$ holds for vertical links. This condition is valid also for the eigenvalue functions $\Lambda_q^{(R)}$ and $\Lambda_q^{(B)}$ assigned to the diagonal links provided that the off-diagonal elements $K_{\alpha\beta}^{'(i)}$ either vanish or are proportional to $K_{zz}^{'(i)}$. The restriction on the off-diagonal elements, $S_z^{max} < D_z^{min}$, is because of the necessary positivity condition for $\Lambda_q = \mathcal{T}_q/c_e t_q^{\star}$. Relations (21)–(24) with (94) yield equal eigenvalue functions for the coordinate and diagonal links when the diffusion tensor is isotropic.

The picture on the left in Fig. 8 demonstrates the solution $h(z)/h^{(I)}$, where $h^{(I)}$ is an exact interface value. The solution is exact for any ratio of vertical

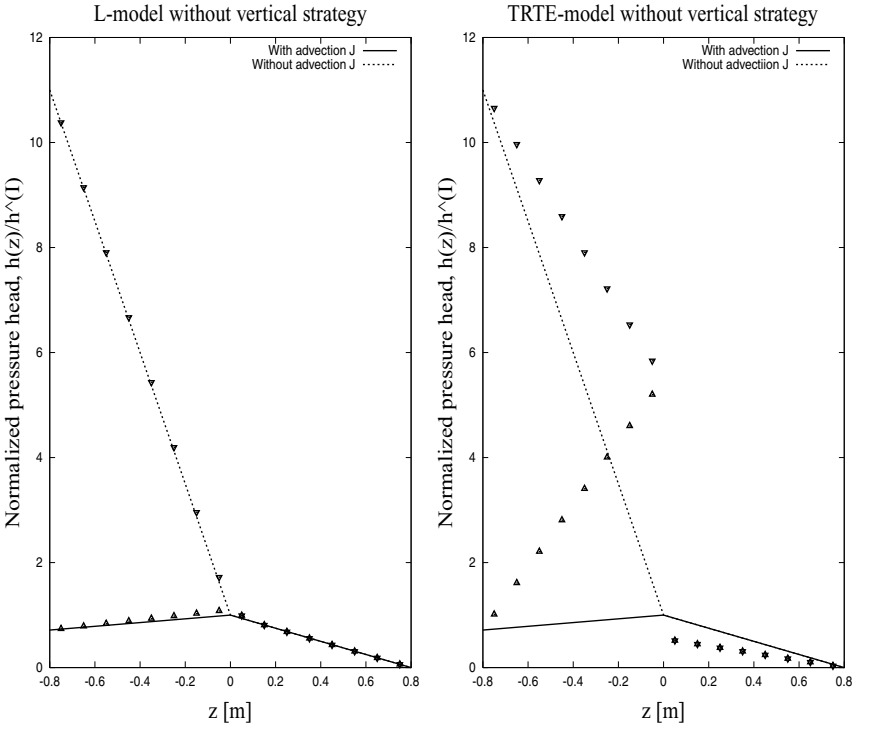

Fig. 9. Vertical flow is computed with the implicit interface tracking. Same data as for the previous figure **but the vertical strategies (94), (95) are not used**. **Left:** L-model is applied with $\Lambda_q^{(R)} = \Lambda_q^{(B)} = \frac{1}{2}$ for all diagonal links, and $\Lambda_q^{(R)} = \frac{1}{2}$, $\Lambda_q^{(B)} = 7\frac{1}{4}$ for the vertical links such that the solution $\Lambda_q^{(R)}/\Lambda_q^{(B)} = r_z$ is not satisfied. **Right:** TRT-E-model is applied with $\Lambda_o^{(R)} = \Lambda_o^{(B)} = 5$ such that the condition (91) is not satisfied.

components provided that the condition $\Lambda_q^{(R)}/\Lambda_q^{(B)} = r_z$ is satisfied. In principle, when the piece-wise constant advection term is present, $\vec{\mathbf{J}}^{(i)} = -\mathbf{K}'^{(i)} \cdot \vec{\mathbf{I}}_z$, the flux condition in (93) should incorporate $J_q^{(i)}$. The solution for $\Lambda_q^{(R)}/\Lambda_q^{(B)}$ will then depend on the effective r_z-value. We find however that using the eigenvalue strategy (94), the solution remains exact even when the advection term is present. This means that the accommodation terms,[16] appearing to link the discontinuous $J_q^{(i)}$ values, have no impact on the diffusion variable and its gradients. When $\Lambda_q^{(R)}/\Lambda_q^{(B)} \neq K_{zz}^{'(R)}/K_{zz}^{'(B)}$ for some interface links, the solution is no longer exact.

We mention, that the uniform horizontal flow needs to chose equal values, $\Lambda_q^{(B)} = \Lambda_q^{(R)}$, for the *diagonal links* (cf. rel. (93) where $\Lambda_q^{(R)}\partial_\alpha \bar{\mathcal{D}}^{(R)} = \Lambda_q^{(B)}\partial_\alpha \bar{\mathcal{D}}^{(B)}$, $r_\alpha = 1$, $\alpha = \{x, y\}$). Obviously, the "vertical" and "horizontal" constraints can

not be satisfied simultaneously for the diagonal links. This problem is investigated in Ref. 27. The picture on the left in Fig. 9 shows one example. Here, the eigenvalue functions follow the "horizontal" strategy such that $\Lambda_q^{(R)} = \Lambda_q^{(B)}$ for the diagonal links and no one interface link satisfies the condition $\Lambda_q^{(R)}/\Lambda_q^{(B)} = r_z$.

TRT-E Model (anisotropic weights, isotropic eigenvalues): the equality of the equilibrium weights would restrict the heterogeneity of the anisotropic properties. Constructing the exact population solution for the vertical heterogeneous flow (to be reported in Ref. 16), one can show that the coupling terms have no impact on the diffusion variable and its gradients when all $\Lambda_o^{(i)}$ are proportional to $K_{zz}^{'(i)}$ (β_E is the coefficient of proportionality restricted by stability conditions on the equilibrium weights (see Refs. 23, 26):

$$\Lambda_o^{(i)} = \beta_E K_{zz}^{'(i)}, \quad \text{then } \beta_E{}^{-1} = 2\sum_{q\in I} E_q^{(i)} = 2\sum_{q\in I} E_q^{(i)} C_{qz}^2,$$

$$\beta_E \geq \max_i \left\{ \frac{K^{max(i)}}{K_{zz}^{'(i)}} \right\}, \quad K^{max(i)} = \max_{\alpha=1,\ldots,d} \{K_{\alpha\alpha}^{'(i)}\}, \tag{95}$$

Using rel. (95) for $\Lambda_o^{(i)}$, the weights are continuous only when the two tensors, $\mathbf{K}^{'(R)}$ and $\mathbf{K}^{'(B)}$ are proportional. The model nevertheless keeps the exact solutions, with and without advection and regardless of the heterogeneity/anisotropy of the diagonal and off-diagonal elements. When the necessary condition (91) is not satisfied, the obtained equilibrium distributions are discontinuous on the interface. The picture on the right in Fig. 9 demonstrates an example: using equal eigenvalue functions, $\Lambda_o^{(R)} = \Lambda_o^{(B)}$, the jump in diffusion coefficients is matched with the equilibrium weights. The diffusion variable then undergoes a jump on the interface: $h^{(R)}/h^{(B)} = K_{zz}^{'(B)}/K_{zz}^{'(R)} = 10$.

This examples demonstrates that working with the discontinuous equilibrium weights, one should be much more careful with the choice of the free parameters. When the weights are continuous, the "risk" consists only in a possible shift (for non-linear solutions) of the effective interface position, but at leading order the continuity relations are valid on the interface.

Parabolic solutions. We construct the parabolic solutions inspired by two phase Poiseuille flow:

$$\partial_{\alpha'} K_{\alpha\beta}^{'(R)} \partial_{\beta'} h' = -M^{(R)}, \quad z' < z^{(I)},$$
$$\partial_{\alpha'} K_{\alpha\beta}^{'(B)} \partial_{\beta'} h' = -M^{(B)}, \quad z' > z^{(I)}, \tag{96}$$

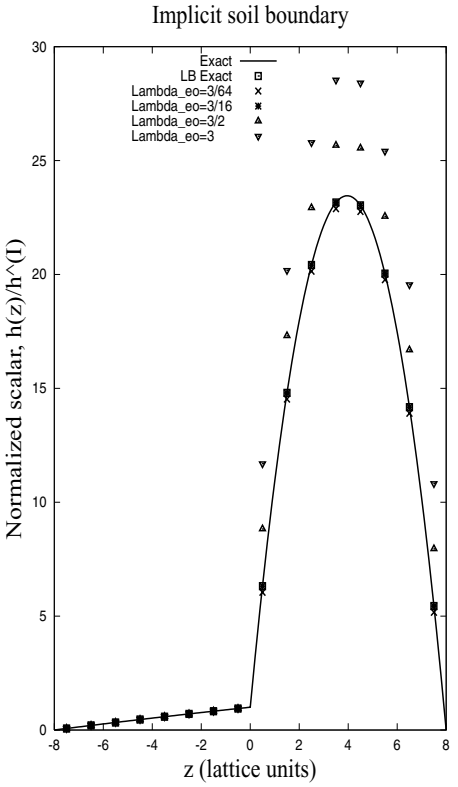

Fig. 10. Piece-wise parabolic distribution $h(z)$ for $K_{zz}^{'(R)}/K_{zz}^{'(B)} = 100$ and $M^{(B)}/M^{(R)} = 10$ is computed with the different combinations $[\Lambda_e\Lambda_o]^{(i)}$, $[\Lambda_e\Lambda_o]^{(R)} = [\Lambda_e\Lambda_o]^{(B)}$. Anti-bounce-back condition is applied on the solid boundaries. **Implicit interface** lies in the middle between two grid node rows. *The solution is exact when* $[\Lambda_e\Lambda_o]^{(i)}$ *are computed with rel.* (99). Data: $K_{zz}^{'(R)} = \frac{1}{6}$, $\Lambda_o^{(R)} = \frac{1}{2}$, $\Lambda_o^{(B)} = \frac{1}{2} \times 10^{-2}$, $M^{(R)} = 1$, $s_q^m = \frac{1}{3}$ when $q \neq 0$.

with interface conditions (33) and Dirichlet boundary conditions $h'(\pm H) = 0$ (as an example). For these solutions, one can write $\mathcal{Q}_q^+ = -s_q^m \Lambda_q \partial_q^2 f_q^{\text{eq.}+}$ when $C_{qz} \neq 0$ where s_q^m are some weight factors such that $\sum_{q=1}^{Q-1} s_q^m \Lambda_q \partial_q^2 f_q^{\text{eq.}+} = -M$.

Assuming a constant advective term, then $p_q^{[1]} = 0$, $p_q{}^{[2]}$ is given by rel. (36) and the last term in interface continuity condition (40), neglected by rel. (90), becomes

$$-\Lambda_e p_q^{[2]} + \frac{1}{2}\mathcal{Q}_q^+ = a_q \partial_q^2 f_q^{\text{eq.}+}, \quad a_q = \Lambda_{eq}(1 - s_q^m) - \frac{s_q^m}{2}\Lambda_q, \quad q \in I. \tag{97}$$

In particular, for isotropic media, $K'^{(i)}_{\alpha\beta} = K'^{(i)}\delta_{\alpha\beta}$, $M^{(i)} = -K'^{(i)}\partial_z^2 h'^{(i)}$, one can put:

$$E_q^{(i)} = c_e t_q^\star, \quad \Lambda_q^{(i)} = \Lambda_o^{(i)} = K'^{(i)} c_e^{-1}, \quad \mathcal{Q}_q^{+(i)} = s_q^m t_q^\star M^{(i)}, \quad \sum_{q=0}^{Q-1} s_q^m t_q^\star = 1 \tag{98}$$

When $[\partial_q^2 f_q^{\text{eq.}+}]^{(R)} = [\partial_q^2 f_q^{\text{eq.}+}]^{(B)}$ (e.g. $E_q^{(R)} = E_q^{(B)}$ and the curvatures are equal), the LB solution is exact on the interface when the pre-factors are equal, $a_q^{(R)} = a_q^{(B)}$. Otherwise, rel. (97) expands the continuity relations to second order if, for the interface links $q \in I$:

$$a_q^{(i)} = \frac{1}{8} \ : \ \Lambda_{eq}^{(i)} = [\Lambda_e \Lambda_q]^{(i)} = \left[\frac{1}{8(1 - s_q^m)} + \frac{\Lambda_q s_q^m}{2(1 - s_q^m)} \right]^{(i)}, \quad 0 \le s_q^m < 1. \tag{99}$$

In contrast to the Poiseuille flow solution (61), not only the diagonal links but also the vertical links should satisfy condition (99). The TRT-E model ($\Lambda_q^{(i)} = \Lambda_o^{(i)}$) can satisfy rel. (99) when s_q^m are equal for all interface links. Under this condition, the L- model can satisfy them only when Λ_q values are equal for interface links inside each soil. When $s_q^m = \frac{1}{3}$, $q \neq 0$ and $\Lambda_q \to 0$, solution (99) coincides with rel. (61). We set $\mathcal{Q}_q^{+(i)} = \frac{1}{3} t_q^\star M^{(i)}$, $q \neq 0$, for all computations below. The second term in rel. (99) which differs from rel. (61) appears since the momentum, J_α, is redefined with the half forcing but the diffusion variable is not redefined with half the source quantity.

Substituting the second order expansion (34), (36) into the anti-bounce-back condition (92), one finds that it localizes, for the parabolic solution, the solid boundaries midway between $\vec{\mathbf{r}}_\text{b}$ and $\vec{\mathbf{r}}_\text{b} + \vec{\mathbf{C}}_q$ when condition (99) is satisfied. Therefore, condition (99) maintains exactly both, boundary and interface, second order conditions. Figure 10 illustrates the combined error due to the anti-bounce-back and inexact matching of the interface continuity conditions. Likewise for other situations, the error is small when $[\Lambda_e \Lambda_q]^{(i)}$ lies below its exact value (99) and increases drastically with $[\Lambda_e \Lambda_q]^{(i)}$. One can compare these results with the analogous ones for two phase Poiseuille flow shown in Fig. 4.

5.1.4. Vertical Three-layered Drainage System

The analysis above is formally restricted to steady state solutions. However, preliminary experiments with the transient solutions to Richard's equation confirm its validity for them as well. Fig. 12 shows the time evolution in a three-layered drainage tube, a tough example borrowed from Marinelli and Durnford.[38] The plots are given for the pressure head $h(z)$, effective water content variable $\tilde{\theta}(z)$,

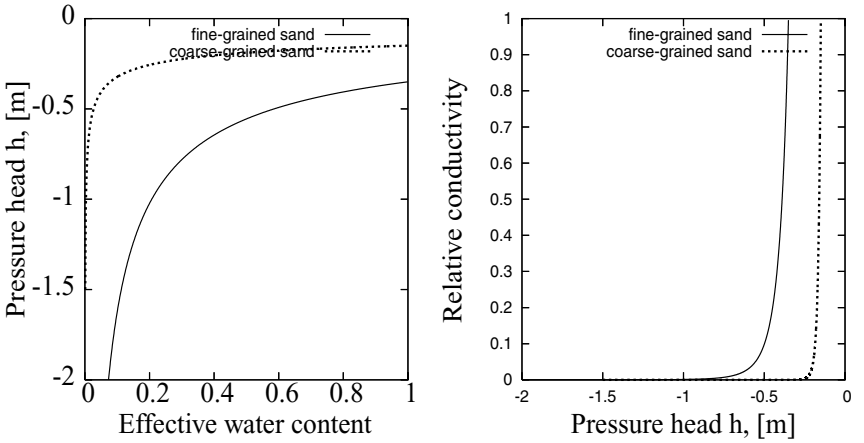

Fig. 11. Prescribed retention function $h(\tilde{\theta})$ (left picture) and relative hydraulic conductivity function $K_r(\tilde{\theta}) = K(\tilde{\theta})/K_s$ (right picture) are obtained with the BCM model: **fine-grained sand**: $K_s = 3.528^{-3} m/hour, \theta_s = 0.35, \theta_r = 0.07, \lambda = 1.5, h_s = -0.35\ m$; **medium-grained sand**: $K_s = 3.528 \times 10^{-1}\ m/hour, \theta_s = 0.35, \theta_r = 0.035, \lambda = 3, h_s = -0.15\ m$.

$\tilde{\theta} = \frac{\theta - \theta_s}{\theta_s - \theta_r}$, and Darcy's velocity $u_z(z)$. The column contains medium-grained sand in the middle and fine-grained sand at the top and bottom. The soil is described with the BCM (Brooks and Corey[3]-Mualem[40]) constitutive relations plotted in Fig. 11: $h(\tilde{\theta}) = h_s \tilde{\theta}^{-1/\lambda}$, $\lambda > 0$, $K_r(h) = (h/h_s)^{-(\lambda(l+2)+2)}$, with $l = 0.5$ as the pore connectivity parameter.

The mixed LB formulation is applied on an equidistant grid using space step $\delta_z = 1/150\ m$ and time step $\delta_t = 24\ s$. The reference solution (dotted line) is computed following the "semi-analytical approach",[38] implemented in the form described in Ref. 26. The reference method is based on the 1D adaptive space step-size control Runge-Kutta (RKA) algorithm and the implicit time discretization. Here, the minimum RKA space step $\delta_z^{min} \approx 10^{-8} - 10^{-7}\ m$ and $\Delta_t = 10800\ s$. We show in Ref. 26 that the RKA method needs extremely small space steps to accurately compute the jumps of the pressure gradients at the interfaces. The obtained solutions differ mainly at the initial stage, when the flow changes rapidly from the saturated one to the unsaturated one and the LB "compressible" effect in the saturated zone is not completely reduced ($\partial_t h(t) \neq 0$). The results confirm that the pressure head space distribution is continuous, whereas the conserved quantity, the water content, undergoes jumps on the soil boundaries.

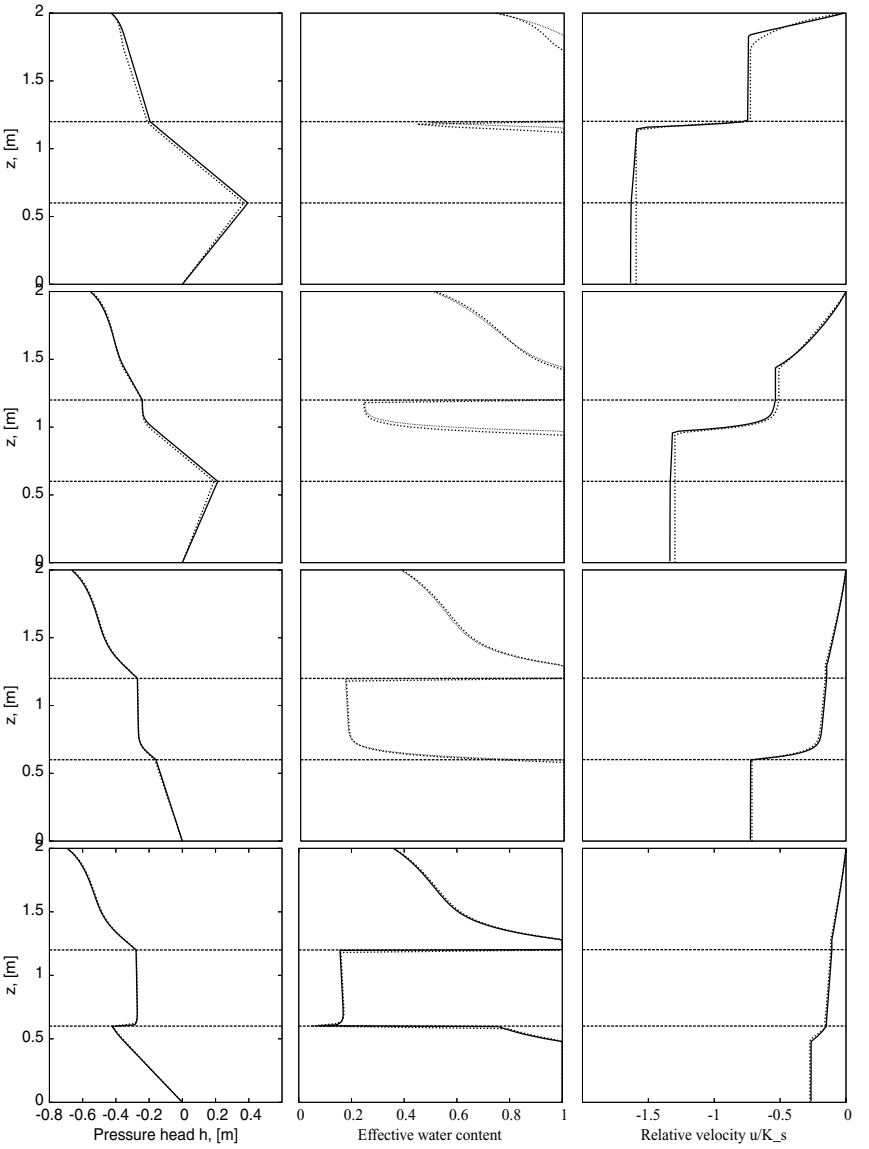

Fig. 12. The picture shows the progression at time $t/3600 = 3, 15, 57, 72\ s$, of the vertical drainage in a three-layered soil tube of 2 m length when the pressure head $h = 2\ m$ at the base is suddenly reduced to the atmospheric value at $t = 0$. The solutions are computed with the mixed LB formulation (solid line) and the "semi-analytical approach" (dotted line).

5.2. Explicit Interface: Collision Components

We analyze rel. (48)–(49) derived for the explicit interface $z = z^{(I)}$, located at the grid nodes midway between the nodes with "red" and "blue" collisions (see Fig 2).

5.2.1. Advective-diffusive fluxes

Let us first consider Eq. (49). For the interface mass source

$$\mathcal{Q}_q^{+(I)} = \frac{1}{2}(\mathcal{Q}_q^{+(R)} + \mathcal{Q}_q^{+(B)}), \tag{100}$$

the source terms vanish in Eq. (49). If we set

$$p_q^{(I)} = \frac{1}{2}(p_q^{(R)} + p_q^{(B)}), \tag{101}$$

then rel. (49) reduces to rel. (89). We use it below in the form:

$$f_q^{\text{eq.}-(R)} - f_q^{\text{eq.}-(B)} = \Lambda_q^{(R)} m_q^{(R)} - \Lambda_q^{(B)} m_q^{(B)}, \quad m_q = \lambda_q^- f_q^{\text{ne.}-}. \tag{102}$$

Again, the sum over the interface links yields the continuity of the normal flux component. Let us now consider rel. (101). If the free eigenvalues are equal, $\lambda_e^{(I)} = \lambda_e^{(R)} = \lambda_e^{(B)}$, then Eq. (101) becomes

$$f_q^{\text{ne.}+(I)} = \frac{1}{2}(f_q^{\text{ne.}+(R)} + f_q^{\text{ne.}+(B)}). \tag{103}$$

According to the definitions in (47), rel. (103) implies:

$$f_q^{\text{eq.}+(I)} = \frac{1}{2}(f_q^{\text{eq.}+(R)} + f_q^{\text{eq.}+(B)}) + \frac{1}{2}(f_q^{-(R)} - f_q^{-(B)}). \tag{104}$$

Substituting rel. (102) for $f_q^{\text{eq.}-(R)} - f_q^{\text{eq.}-(B)}$, then

$$f_q^{-(R)} - f_q^{-(B)} = (f_q^{\text{ne.}-(R)} - f_q^{\text{ne.}-(B)}) - \\ ((f_q^{\text{ne.}-(R)} + \frac{1}{2}m_q^{(R)}) - (f_q^{\text{ne.}-(B)} + \frac{1}{2}m_q^{(B)})) = \frac{1}{2}(m_q^{(B)} - m_q^{(R)}) \tag{105}$$

and rel. (104) becomes

$$f_q^{\text{eq.}+(I)} = \frac{1}{2}(f_q^{\text{eq.}+(R)} + f_q^{\text{eq.}+(B)}) + \frac{1}{4}(m_q^{(B)} - m_q^{(R)}). \tag{106}$$

This means that the equilibrium symmetric part will differ from the continuous values $f_q^{\text{eq.}+(R)} = f_q^{\text{eq.}+(B)}$ unless the soil is homogeneous ($m_q^{(B)} = m_q^{(R)}$). Section 5.2.4 further comments on this relation.

5.2.2. Interface diffusion coefficients

We consider now Eq. (48). We define first $f_q^{\text{eq.}-(I)}$:

$$f_q^{\text{eq.}-(I)} = \frac{1}{2}\left(f_q^{\text{eq.}-(R)} + f_q^{\text{eq.}-(B)}\right),\ q \in I. \tag{107}$$

Using this definition, we split $f_q^{\text{ne.}-(I)}$ into two parts:

$$f_q^{\text{ne.}-(I)} = f_q^{\text{ne.}-(I)[1]} + f_q^{\text{ne.}-(I)[2]},$$

$$f_q^{\text{ne.}-(I)[1]} = \frac{1}{2}\left(f_q^{\text{ne.}-(R)} + f_q^{\text{ne.}-(B)}\right), \tag{108}$$

$$f_q^{\text{ne.}-(I)[2]} = \frac{1}{2}\left(f_q^{+(R)} - f_q^{+(B)}\right). \tag{109}$$

If we set

$$\lambda_q^{-(I)} f_q^{\text{ne.}-(I)[1]} = \frac{1}{2}\left(m_q^{(R)} + m_q^{(B)}\right) \quad \text{and} \tag{110}$$

$$\lambda_q^{-(I)} f_q^{\text{ne.}-(I)[2]} = \left(\Lambda_e^{(R)} p_q^{(R)} - \Lambda_e^{(B)} p_q^{(B)}\right) + \frac{1}{2}\left(\mathcal{Q}_q^{+(B)} - \mathcal{Q}_q^{+(R)}\right), \tag{111}$$

then Eq. (48) becomes

$$f_q^{\text{eq.}+(R)}(\vec{\mathbf{r}}^{(I)}) = f_q^{\text{eq.}+(B)}(\vec{\mathbf{r}}^{(I)}) + O(\varepsilon^3), \quad q \in I. \tag{112}$$

This condition states the continuity of the diffusion variable when the equilibrium weights are continuous. The necessary condition is again given by rel. (91), just as for an implicit interface. Replacing $f_q^{\text{ne.}-(I)[1]}$ by its definition (108), and $m_q^{(B)}/m_q^{(R)}$ by r_q, we obtain from Eq. (110):

$$\text{L}: \Lambda_q^{(I)} = \frac{\Lambda_q^{(B)} r_q + \Lambda_q^{(R)}}{r_q + 1}, \quad \text{where} \quad r_q = m_q^{(B)}/m_q^{(R)}, q \in I,$$

$$\text{TRT-E}: \Lambda_o^{(I)} = \frac{\Lambda_o^{(B)} r_e + \Lambda_o^{(R)}}{r_e + 1}, \quad \text{where} \quad r_e = \sum_{q\in I} m_q^{(B)} / \sum_{q\in I} m_q^{(R)}. \tag{113}$$

They may reduce to harmonic mean solutions:

$$\text{L}: \Lambda_q^{(I)} = \frac{2\Lambda_q^{(B)}\Lambda_q^{(R)}}{\Lambda_q^{(B)} + \Lambda_q^{(R)}}, \quad \text{if} \quad \frac{\Lambda_q^{(R)}}{\Lambda_q^{(B)}} = r_q, \quad q \in I,$$

$$\text{TRT-E}: \Lambda_o^{(I)} = \frac{2\Lambda_o^{(B)}\Lambda_o^{(R)}}{\Lambda_o^{(B)} + \Lambda_o^{(R)}}, \quad \text{if} \quad \frac{\Lambda_o^{(R)}}{\Lambda_o^{(B)}} = r_e. \tag{114}$$

According to rel. (21), the vertical diffusion interface coefficients $K_{zz}^{'(I)}$ are:

$$\mathrm{L}: K_{zz}^{'(I)} = 2c_e \sum_{q\in I} \Lambda_q^{(I)} t_q^{\star}, \quad \text{if } E_q^{(i)} = c_e t_q^{\star}, \quad q \in I, (i) = \{(R), (B), (I)\}$$

$$\text{TRT-E}: K_{zz}^{'(I)} = \beta_E \Lambda_o^{(I)}, \qquad {\beta_E}^{-1} = 2\sum_{q\in I} E_q^{(i)}. \tag{115}$$

When, for the L-model, $r_q = r_e, \forall q \in I$, then for both models,

$$K_{zz}^{'(I)} = \frac{K_{zz}^{'(B)} r_e + K_{zz}^{'(R)}}{r_e + 1}, \tag{116}$$

and for the vertical strategies (94), (95), $K_{zz}^{'(I)}$ becomes equal to the harmonic mean value:

$$K_{zz}^{'(I)} = \frac{2K_{zz}^{'(R)} K_{zz}^{'(B)}}{K_{zz}^{'(R)} + K_{zz}^{'(B)}}, \quad \text{if} \quad r_e = r_z = \frac{K_{zz}^{'(R)}}{K_{zz}^{'(B)}}. \tag{117}$$

This solution coincides with the commonly used vertical approximation for the inverse of the resistance in case of the direct discretization methods (e.g., in Ref. 1). For the diffusion equation with the piece-wise constant coefficients, the harmonic mean interface approximation follows from the exact flux balance condition (e.g., in Ref. 53).

5.2.3. Free collision parameters

Substituting condition (109) with rel. (112) into condition (111), we obtain:

$$\frac{\lambda_q^{-(I)}}{2}\left(\frac{p_q^{(R)}}{\lambda_e^{(R)}} - \frac{p_q^{(B)}}{\lambda_e^{(B)}}\right) = \left(\Lambda_e^{(R)} p_q^{(R)} - \Lambda_e^{(B)} p_q^{(B)}\right) + \frac{\mathcal{Q}_q^{+(B)} - \mathcal{Q}_q^{+(R)}}{2}. \tag{118}$$

When the free eigenvalues are equal and we substitute $\mathcal{Q}_q^{+(i)} = -s_q^m [\Lambda_q \partial_q^2 f_q^{\mathrm{eq.}+}]^{(i)}$, the solution is

$$\lambda_e^{(B)} = \lambda_e^{(R)} = \lambda_e^{(I)}, \quad \text{if} \quad \mathcal{Q}_q^{+(R)} = \mathcal{Q}_q^{+(B)}, \quad q \in I,$$

$$\Lambda_{eq}^{(I)} = \Lambda_e^{(I)} \Lambda_q^{(I)} = \frac{1}{4(1 - s_q^m)} + \frac{\Lambda_q^{(I)} s_q^m}{2(1 - s_q^m)}, \quad q \in I,$$

$$\text{i.e. } \lambda_e^{(I)} = \lambda_e^{(B)} = \lambda_e^{(R)} = -(2 + \lambda_q^{-(I)})(1 - s_q^m), \quad \text{if} \quad \mathcal{Q}_q^{+(R)} \neq \mathcal{Q}_q^{+(B)}. \tag{119}$$

Here again, all interface links should satisfy rel. (119). When $s_q^m = \frac{1}{3}, q \neq 0$, and $\Lambda_q^{(I)} \to 0$, rel. (119) becomes equal to sol. (80). When s_q^m are equal for interface links, solution (119) is available only when $\Lambda_q^{(I)}$ are also equal for all interface

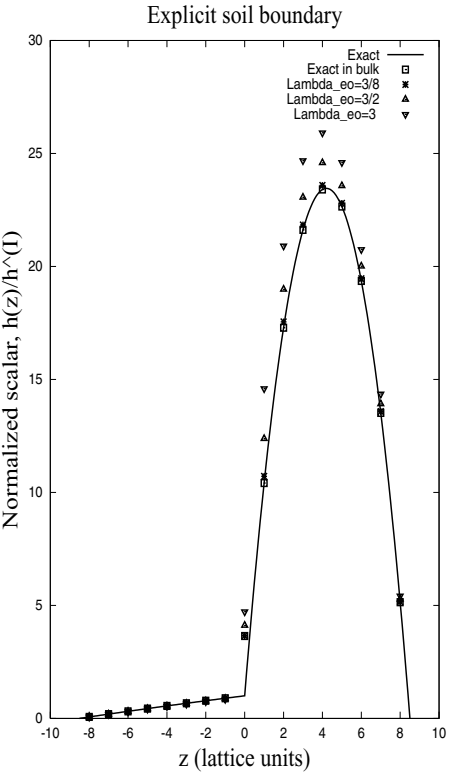

Fig. 13. Piece-wise parabolic distribution $h(z)$ for $K_{zz}^{'(R)}/K_{zz}^{'(B)} = 100$ and $M^{(B)}/M^{(R)} = 10$ is computed with different combinations $[\Lambda_e\Lambda_o]^{(I)}$ when $\Lambda_e^{(I)} = \Lambda_e^{(B)} = \Lambda_e^{(R)}$. Exact multi-reflection type boundary conditions are applied for solid walls. The boundary between two soils is located at the grid node row (**explicit tracking**). *The solution is "exact in the bulk"* when $[\Lambda_e\Lambda_o]^{(I)}$ is computed from rel. 119. The data is given in the caption to the Fig. 10.

links. This means that, for such solutions, the L-model is restricted to diagonal tensors, at least using the vertical strategy (94) when $K_{zz}^{'(R)} \neq K_{zz}^{'(B)}$. The TRT-E-model with the vertical strategy (95) may handle exact parabolic solutions for any tensors, owing to Λ_{eo} and accommodation layers.

5.2.4. Summary

Due to exact mass conservation, the normal component of the advective-diffusive flux is continuous on the *computational grid* regardless of the selected interface components. The interface node $\vec{\mathbf{r}}^{(I)}$ will maintain the solutions with the continuous symmetric equilibrium parts, $f_q^{\text{eq.}+(R)} = f_{\bar{q}}^{\text{eq.}+(B)}$ and the continuous

advective-diffusive flux components, $f_q^{\text{eq.}-(R)} + \Phi_q^{(R)} = f_q^{\text{eq.}-(B)} + \Phi_q^{(B)}$, provided that the collision components satisfy conditions (100), (101), (107), for the interface links, and condition (113) for the interface eigenvalue functions. These conditions are, respectively:

$$\mathcal{Q}_q^{+(I)} = \frac{1}{2}\left(\mathcal{Q}_q^{+(R)} + \mathcal{Q}_q^{+(B)}\right), \tag{120}$$

$$p_q^{(I)} = \frac{1}{2}\left(p_q^{(R)} + p_q^{(B)}\right), \tag{121}$$

$$f_q^{\text{eq.}-(I)} = \frac{1}{2}\left(f_q^{\text{eq.}-(R)} + f_q^{\text{eq.}-(B)}\right), \tag{122}$$

$$\text{L} : \Lambda_q^{(I)} = \frac{\Lambda_q^{(B)} r_q + \Lambda_q^{(R)}}{r_q + 1}, \quad r_q = m_q^{(B)}/m_q^{(R)}, \tag{123}$$

$$\text{TRT-E} : \Lambda_o^{(I)} = \frac{\Lambda_o^{(B)} r_e + \Lambda_o^{(R)}}{r_e + 1}, \quad r_e = \sum_{q\in I} m_q^{(B)} / \sum_{q\in I} m_q^{(R)}. \tag{124}$$

The interface eigenvalue functions are represented by harmonic mean values of the corresponding bulk functions when $r_q = \frac{\Lambda_q^{(R)}}{\Lambda_q^{(B)}}$ and $r_e = \frac{\Lambda_o^{(R)}}{\Lambda_o^{(B)}}$. When

$$r_q = r_e = r_z = \frac{K_{zz}^{'(R)}}{K_{zz}^{'(B)}}, \quad q \in I, \tag{125}$$

the vertical interface coefficient $K_{zz}^{'(I)}$ becomes equal to the harmonic mean value of $K_{zz}^{'(R)}$ and $K_{zz}^{'(B)}$ for diffusion problems.

Let us illustrate rel. (121)–(124) for the piece-wise linear distribution $\bar{\mathcal{D}}(s) = h'(z)$ assuming the simplest case, $E_q^{(B)} = E_q^{(R)} = E_q$, $\vec{\mathbf{J}} = 0$. The exact solution arriving at the interface is

$$f_q^{(I)} = E_q\left(h'^{(R)} + \frac{1}{\lambda_q^{-(R)}}\nabla_q h'^{(R)}\right), \quad f_{\bar{q}}^{(I)} = E_q\left(h'^{(B)} + \frac{1}{\lambda_q^{-(B)}}\nabla_{\bar{q}} h'^{(B)}\right),$$
$$p_q^{(R)} = p_{\bar{q}}^{(B)} = 0, \quad q \in I. \tag{126}$$

When $p_q^{(I)} = 0$ according to condition (121), the populations leaving the interface maintain the solution (126) exactly due to the construction of the interface diffusion coefficients, rel. (123)–(124):

$$\tilde{f}_q^{(I)} = E_q\left(h'^{(B)} + \left(\frac{1}{\lambda_q^{-(B)}} + 1\right)\nabla_q h'^{(B)}\right),$$

$$\tilde{f}_{\bar{q}}^{(I)} = E_q \left(h'^{(R)} + \left(\frac{1}{\lambda_q^{-(R)}} + 1 \right) \nabla_{\bar{q}} h'^{(R)} \right), \quad q \in I. \tag{127}$$

However, Eq. (121) then implies rel. (106), which gives here exactly:

$$h'^{(I)} = \frac{1}{2} \left(h'^{(R)} + h'^{(B)} \right) + \delta h', \quad \delta h' = \frac{1}{4} \left(\partial_z h'^{(B)} - \partial_z h'^{(R)} \right). \tag{128}$$

The picture on the right in Fig. 8 demonstrates the solution $h(z)/h^{(I)}$ again obtained using the anti-bounce-back boundary condition. We set $f_q^{\text{eq.}+}(\vec{\mathbf{r}}^{(I)}) = E_q^{(I)} h'^{(I)}$, $h'^{(I)}$ being the interface diffusion variable. As above, it is related linearly to the conserved quantity s: $h'^{(i)} = s^{(i)} H^{\text{eq.}}$, $\{(i) = (R), (B), (I)\}$, using the steady state pressure formulation for the saturated Richard's equation. The interface coefficient $K_{zz}^{'(I)}$ is computed with rel. (117) when $\vec{\mathbf{J}} = 0$ and with the effective r_z-value, $r_z = [\partial_z \bar{\mathcal{D}}^{(B)} / \partial_z \bar{\mathcal{D}}^{(R)}](\vec{\mathbf{r}}^{(I)})$, when $\vec{\mathbf{J}} \neq 0$. The eigenvalue strategies (94), (95) are then applied for three "soils" ((R), (B) and (I)). *The obtained solutions are exact away from the interface*. The discrepancy between the equilibrium interface value $h^{(I)}$ and the continuation from the bulk, $h^{(R)}(z^{(I)}) = h^{(B)}(z^{(I)})$, is equal to $\delta h'/\mathcal{L}$, where $\delta h'$ is given by rel. (128).

The parabolic solutions are shown in Fig. 13. They are computed with $\mathcal{Q}_q^{+(i)} = 1/3 t_q^\star M^{(i)}$ and the third order accurate, multi-reflection type boundary conditions from Ref. 24 (Eqs. 25–27 there). The harmonic mean value is assigned for the vertical diffusion coefficient $K_{zz}^{'(I)}$. The TRT-E model with the strategy (95) again maintains exact solutions for any heterogeneous anisotropic properties. When the free eigenvalues satisfy rel. (119), the solution is exact in the bulk and the interface discrepancy $\delta h'/\mathcal{L}$ corresponds exactly to Eq. (128). The plots in Fig. 13 demonstrate the impact of the free eigenvalue combination $[\Lambda_e \Lambda_o]^{(I)}$ on the interface accuracy when $\Lambda_e^{(i)}$ are equal for both phases and the interface. As expected, the second order error increases with Λ_e when the diffusion coefficients are fixed.

6. CONCLUDING REMARKS

We have developed an interface analysis for the link-wise collision operators with discontinuous collision components. Interface closure relations have first been established for the symmetric and anti-symmetric parts of the collision operator, regardless of their physical meaning. Prescribing the equilibrium function, they can be used to check the continuity properties of the solutions, both for the hydrodynamic and AADE equations. With the parity argument at hand, we reveal the analogy of their interface behavior. The analysis then focused on two-phase

microscopic flow (without surface tension) and variably saturated Darcy's flows in a stratified anisotropic heterogeneous aquifer.

For the *hydrodynamic* modeling with the *implicit* interface tracking, the effective interface, where the pressure, momentum and tangential shear stress tensor components are continuous, is shown to be located midway between the grid nodes with first-order accuracy (exactly for the piece-wise linear momentum distributions). For the *explicit* tracking, the equilibrium function, forcing and relaxation parameters have been derived from the continuity conditions. The harmonic mean value for the interface kinematic viscosity was found to give an exact solution for the transfer of the shear components. When the interface is in the middle between two phases, the Couette solution for the *tangential momentum component* is then matched exactly in the bulk. However, the conserved interface momentum value and the limit bulk values differ in the case of the explicit interface tracking, even when the obtained bulk solution is exact. Accurate extrapolations from the bulk are therefore needed to define the *macroscopic momentum solution* for the interface nodes. Besides that, when distinct fluid densities are modeled via distinct sound velocities c_s^2, $P^{(i)} = c_s^{2(i)}\rho^{(i)}$, the tangential velocity $j_\alpha^{(i)}/\rho^{(i)}$ appears to be discontinuous on the interface. It would be interesting to understand if the continuity of the tangential momentum (and not the velocity) has a practical impact in realistic computations. Another open question is if the alternative LB approaches for distinct fluid densities maintain the continuity of the velocity (and not of the momentum).

For the *Darcy's flow* modeling with *implicit* tracking of soil interfaces, the continuity of the symmetric equilibrium part and the continuity of the advective-diffusive flux link components is set midway between the grid nodes at first-order. The last condition may constrain not only the normal but also the tangential fluxes. For the *explicit* interface tracking, the interface collision components have been derived from the first-order continuity relations. The harmonic mean value for the inverse of the vertical resistance was found to give an exact solution for the vertical flow in a heterogeneous aquifer, provided that the bulk collision components are chosen with some special rules. The deficiency of the explicit tracking appears here as an inconsistency between the interface diffusion variable and its continuation from the bulk.

For both interface approaches, the choice of the diffusion variable, in the homogeneous case conditioned mainly by the robustness of the algorithm, is constrained by the continuity conditions. As an example, the different LB formulations for the Richard's equation (water content based, pressure based, mixed, and the Kirchoff transform based) have been specified and analyzed. The continuity of the diffusion variable may confine the equilibrium weights and restrict the application of the *equilibrium based* approach (E-model) when the anisotropic properties are *heterogeneous*. The alternative approach (L-model), based on the continuous isotropic equilibrium functions and anisotropic sets of the eigenvalue functions,

appears to be much less sensitive to the choice of the free parameters. Their solutions are problem dependent, and, in particular, the exact collision strategies differ for horizontal and vertical flows. This problem is partially solved in Ref. 27 where the interface corrections to the evolution equation enforce the matching of the continuity relations, regardless of the heterogeneity and the anisotropy of the diffusion tensors.

The solutions obtained for the macroscopic interface transport coefficients are consistent with known results for direct discretization methods. Extending the perturbative interface analysis up to second-order, we find special solutions for the free relaxation parameters which enforce the exact interface conditions for parabolic flows (e.g. two phase Poiseuille flow) or for parabolic distributions of the diffusion variable. Combined with the exact boundary conditions, they present ideal exercises for novices. The exact solutions differ in small details for the explicit and implicit interfaces, the hydrodynamic and AADE modeling, but they all restrict free combinations of the eigenvalue functions similarly. Both analytical and numerical results confirm the necessity to assign small enough values for the free eigenvalue combinations, typically $\Lambda_e \Lambda_q < 1$. These constraints should be respected to avoid numerical inaccuracy in the bulk and at the boundaries and interfaces.

ACKNOWLEDGMENTS

The author is grateful to V. Pot, D. d'Humières, F. Verhaeghe and J. Summers for critical reading of the manuscript.

REFERENCES

1. M. Bakker and K. Hemker, Analytic solutions for groundwater whirls in box-shaped, layered anisotropic aquifers, *Adv. Water Resour.* **27**: 1075–1086 (2004).
2. M. Bouzidi, M. Firdaouss and P. Lallemand, Momentum transfer of a Boltzmann-lattice fluid with boundaries, *Phys. Fluids* **13**: 3452–3459 (2001).
3. R. H. Brooks and A. T. Corey, Hydraulic properties of porous media. *Hydrol. Paper No. 3*, Colorado State University, Fort Collins, Colo. 1964.
4. J. M. Buick and C. A. Greated., Gravity in a lattice Boltzmann model. *Phys. Rev. E* **61**: 5307–5320 (2000).
5. J. M. Buick and C. A. Greated, Lattice-Boltzmann modeling of interfacial gravity waves. *Phys. Fluids* **10**(6):1490–1511 (1998).
6. M. Celia, E. Bouloutas and R. Zabra, A general Mass-Conservative Numerical Solution for the Unsaturated Flow Equation. *Water Resour. Res.* **26**: 1483–1496 (1990).
7. S. Chen and G. D. Doolen, Lattice Boltzmann method for fluid flows. *Ann. Rev. J. Fluid Mechanics* **30**: 329–364 (1998).
8. D. A. Edwards, H. Brenner and D. T. Wasan,*Interfacial transport process and rheology*. Butterworth-Heinemann Series in Chemical Engineering, 1991.

9. U. Frisch, D. d'Humières, B. Hasslacher, P. Lallemand, Y. Pomeau and J.P. Rivet,Lattice gas hydrodynamics in two and three dimensions *Complex Sys.* **1**: 649–707 (1987).
10. E. Guyon, J.-P. Hulin and L. Petit, *Hydrodynamique physique*, Inter Editions/Editions du CNRS, Paris, 1991.
11. X. He and L. S. Luo, Lattice Boltzmann Model for the Incompressible Navier-Stokes Equation. *J. Stat. Phys.* **88**: 927–945 (1997).
12. D. d'Humières, Generalized Lattice-Boltzmann Equations. AIAA Rarefied Gas Dynamics: Theory and Simulations. *Progress in Astronautics and Aeronautics* **59**: 450–548 (1992).
13. D. d'Humières, M. Bouzidi and P. Lallemand, Thirteen-velocity three-dimensional lattice Boltzmann model, *Phys. Rev. E* **63**: 066702-1–7 (2001).
14. D. d'Humières, I. Ginzburg, M. Krafczyk, P. Lallemand and L.-S. Luo,Multiple-relaxation-time lattice Boltzmann models in three dimensions. *Phil. Trans. R. Soc. Lond. A* **360**: 437–451 (2002).
15. D. d'Humières and I. Ginzburg, Some analytical results about the stability of Lattice Boltzmann models, in preparation, 2006.
16. D. d'Humières and I. Ginzburg, Knudsen layers in Lattice Boltzmann modeling, in preparation, 2006.
17. I. Ginzbourg. Boundary conditions problems in lattice gas methods for single and multiple phases, PhD, University Paris VI, 1994.
18. I. Ginzbourg and P. M. Adler, Boundary flow condition analysis for the three-dimensional lattice Bolzmann model, *J. Phys. II France* **4**: 191–214 (1994).
19. I. Ginzbourg and P. Adler, Surface Tension Models with Different Viscosities, *Transport Porous Media* **20**: 37–76 (1995).
20. I. Ginzburg and K. Steiner, A free surface Lattice Boltzmann method for modelling the filling of expanding cavities by Bingham fluids, *Phil. Trans. R. Soc. Lond. A* **360**: 453–466 (2002).
21. I. Ginzburg and K. Steiner, Lattice Boltzmann model for free-surface flow and its application to filling process in casting. *J. Comp. Phys.* **185**: 61–99 (2003).
22. I. Ginzburg and D. d'Humières, Multi-reflection boundary conditions for lattice Boltzmann models. *Phys. Rev. E* **68**: 066614-1-30 (2003).
23. I. Ginzburg, Equilibrium-type and Link-type Lattice Boltzmann models for generic advection and anisotropic-dispersion equation, *Adv. Water Resour.* **28**: 1171–1195 (2005).
24. I. Ginzburg, Generic boundary conditions for Lattice Boltzmann models and their application to advection and anisotropic-dispersion equations. *Adv. Water Resour.* **28**: 1196–1216 (2005).
25. I. Ginzburg and J.-P. Carlier and C. Kao, Lattice Boltzmann approach to Richards' equation, in: *Computational methods in water resources*. Proc. of the CMWR XV, Chapen Hill, USA, 2004, eds. C. T. Miller, Elsevier, pp. 583–597, 2004.
26. I. Ginzburg, Variably saturated flow described with the anisotropic Lattice Boltzmann methods. *J. Comput. Fluids* **35**(8/9):831–848 (2006).
27. I. Ginzburg and D. d'Humières, Lattice Boltzmann and analytical solutions for flow process in anisotropic heterogeneous stratified aquifers, submitted to Advances in Water Resour., 2006.
28. A. K. Gunstensen, D. H. Rothmann, S. Zaleski and G. Zanetti, Lattice Boltzmann model of immiscible fluids. *Phys. Rev. A* **43**: 4320–4327 (1991).
29. Z. Guo, C. Zheng, and B. Shi, Discrete lattice effects on the forcing term in the lattice Boltzmann method, *Phys. Rev. E* **65**: 066308-1-6 (2003).
30. D. Grunau, S. Chen and K. Eggert, A lattice Boltzmann model for multiphase fluid flows. *Phys. Fluids A5* 2557–2562 1993.
31. X. He, S. Chen and R. Zhang, A Lattice Boltzmann scheme for incompressible multiphase flow and its application in simulation of Rayleigh-Taylor instability. *J. Comput. Phys.* **152**: 642–663 (1999).
32. S. Hou, X. Shan, Q. Zou, G.D. Doolen and W.E. Soll, Evaluation of Two Lattice Boltzmann Models for Multiphase Flows. *J. Comput. Phys.* **138**: 695–713 (1996).

33. T. Inamuro, N. Konishi and F. Ogino, A Galilean invariant model of the lattice Boltzmann method for multiphase fluid flows using free-energy approach. *Comput. Phys. Commun.* **129**: 32–45 (2000).
34. A. J. C. Ladd, Numerical simulations of particulate suspensions via a discretized Boltzmann equation. Part 2. Numerical results. *J. Fluid Mech.* **271**: 311–339 (1994).
35. D. Kehrwald, *Numerical analysis of immiscible lattice BGK*, PhD. diss, UNI Kaiserslautern, Germany, 2002.
36. C. Körner, M. Thies, T. Hoffmann, N. Thürey and U. Rüde, Lattice Boltzmann Model for Free Surface flow for modeling Foaming, *J. Stat. Phys.* **121**: 179–197 (2005).
37. P. Lallemand and L.-S. Luo, Theory of the lattice Boltzmann method: Dispersion, dissipation, isotropy, Galilean invariance, and stability. *Phys. Rev. E* **61**: 6546–6562 (2000).
38. F. Marinelli and D. S. Durnford, Semianalytical solution to Richards' Equation for layered porous media. *J. Irrigat. Drainage Eng.* **124**(6):290–299 (1998).
39. C. T. Miller, C. Abhishek, A. B. Sallerson, J. F. Prins and M. W. Farthing, A comparison of computational and algorithmic advances for solving Richards' equation, "Computational methods in water resources". C.T. Miller (ed.), *Proc. of the CMWR XV, June 13–17*, Chapel Hill, NC, USA, **2**: pp. 1131–1145, Elsevier, 2004.
40. Y. Mualem, A new model for predicting the hydraulic conductivity of unsaturated porous media, *Water Resour. Res.* **12**: 513–522 (1976).
41. X. Nie, Y.-H. Qian, G. D. Doolen and S. Chen, Lattice Boltzmann simulation of the two-dimensional Rayleigh-Taylor instability. *Phys. Rev. E* **58**: 6861–6864 (1998).
42. Y. Qian, D. d'Humières and P. Lallemand, Lattice BGK models for Navier-Stokes equation. *Europhys. Lett.* **17**: 479–484 (1992).
43. C. Pan, M. Hilpert and C. T. Miller, Lattice Boltzmann simulation of two-phase flow in porous media, *Water Resour. Res.* **40**(1):W01501:1–14 (2004).
44. C. Pan, L. Luo and C. T. Miller, An evaluation of lattice Boltzmann schemes for porous media simulations, *J. Comput. Fluids* **35**(8/9):898–909 (2006).
45. U. D'Ortona, D. Salin, M. Cieplak, R. B. Rybka and J. R. Banavar, Two-color nonlinear Boltzmann cellular automata: Surface tension and wetting, *Phys. Rev. E* **51**: 3718–3751 (1995).
46. D. Raabe, Overview of the lattice Boltzmann method for nano-and microscale fluid dynamics in matherial science and engineering, *Model. Simul. Mater. Sci. Eng.* **12**: R13–R46 (2004).
47. L. O. E. dos Santos and P. C. Philippi, Lattice-gas model based on field mediators for immiscible fluids, *Phys. Rev. E* **65**: 046305-1-8 (2002).
48. X. Shan and G. D. Doolen, Multi-component lattice-Boltzmann model with interparticle interaction, *J. Stat. Phys.* **81**(1/2):379–393 (1995).
49. X. Shan and G. Doolen, Diffusion in a multicomponent lattice Boltzmann equation model. *Phys. Rev. E* **54**: 3614–3620 (1996).
50. M. R. Swift, E. Orlandini, W. R. Osborn and J. M. Yeomans, Lattice Boltzmann simulation of liquid-gas and binary fluid systems, *Phys. Rev. E* |bf 54: 5041–5052 (1996).
51. D. H. Rothman and S. Zaleski, *Lattice Gas Dynamics Automata—Simple Model for Complex Hydrodynamics,* Cambridge University Press, ISBN: 0-521-55201-X, 1997.
52. P. J. Ross, Modeling soil water and solute transport-Fast, simplified numerical solutions *Agronomy J.* **95**: 1352–1361 (2003).
53. A. Tichonov and A. Samarsky, *Equations of mathematical physics.* Nauka, Moscow, 1977.
54. J. Tölke, Die Lattice Boltzmann Methode für Mehrphasenströmungen. PhD.diss LS Bauinformatik, TU, München, Germany, 2001.
55. J. Tölke, M. Krafczyk, M. Schulz and E. Rank, Lattice Boltzmann simulations of binary fluid flow through porous media, *Phil. Trans. R. Soc. Lond. A* **360**: 535–545 (2002).
56. H.-J. Vogel, J. Tölke, V. P. Schulz, M. Krafczyk and K. Roth, Comparison of Lattice-Boltzmann Model, a Full-Morphology Model, and a Pore Network Model for Determining Capillary Pressure-Saturation Relationships, *Vadoze Zone J.* **4**: 380–388 (2005).

57. X. Zhang, A. G. Bengough, L. K. Deeks, J. W. Crawford and I. M. Young, A lattice BGK model for advection and anisotropic dispersion equation. *Adv. Water Resour.* **25**: 1–8 (2002a).
58. X. Zhang, A. G. Bengough, L. K. Deeks, J. W. Crawford and I.M. Young, A novel three-dimensional lattice Boltzmann model for solute transport in variably saturated porous media, *Water Resour. Res.* **38**: 1–10 (2002b).